Human Molecular Genetics, 2013, Vol. 22, No. 20 **4084–4101**
doi:10.1093/hmg/ddt258
Advance Access published on June 4, 2013

The DcpS inhibitor RG3039 improves survival, function and motor unit pathologies in two SMA mouse models

Rocky G. Gogliotti[1,2,†], Herminio Cardona[2,†], Jasbir Singh[3,†], Sophie Bail[4], Carina Emery[1,2], Nancy Kuntz[1,5], Michael Jorgensen[2], Madel Durens[4], Bing Xia[6], Courtenay Barlow[1,2], Christopher R. Heier[1,2], Heather L. Plasterer[6], Vincent Jacques[6], Megerditch Kiledjian[4], Jill Jarecki[7], James Rusche[6] and Christine J. DiDonato[1,2,*]

[1]Department of Pediatrics, Feinberg School of Medicine, Northwestern University, Chicago, IL, USA [2]Human Molecular Genetics Program, Ann & Robert H. Lurie Children's Hospital of Chicago Research Center, Chicago, IL, USA [3]JASIN Discovery Solutions, Inc., Naperville, IL, USA [4]Department of Cell Biology and Neuroscience, Rutgers University, USA [5]Division of Neurology, Ann & Robert H. Lurie Children's Hospital of Chicago, Chicago, IL, USA [6]Repligen Corporation, Waltham, MA, USA [7]Families of SMA, Elk Grove Village, IL, USA

Received March 25, 2013; Revised May 9, 2013; Accepted May 28, 2013

Spinal muscular atrophy (SMA) is caused by insufficient levels of the survival motor neuron (SMN) protein due to the functional loss of the *SMN1* gene and the inability of its paralog, *SMN2*, to fully compensate due to reduced exon 7 splicing efficiency. Since SMA patients have at least one copy of *SMN2*, drug discovery campaigns have sought to identify *SMN2* inducers. C5-substituted quinazolines increase *SMN2* promoter activity in cell-based assays and a derivative, RG3039, has progressed to clinical testing. It is orally bioavailable, brain-penetrant and has been shown to be an inhibitor of the mRNA decapping enzyme, DcpS. Our pharmacological characterization of RG3039, reported here, demonstrates that RG3039 can extend survival and improve function in two SMA mouse models of varying disease severity (Taiwanese 5058 Hemi and 2B/− SMA mice), and positively impacts neuromuscular pathologies. In 2B/− SMA mice, RG3039 provided a >600% survival benefit (median 18 days to >112 days) when dosing began at P4, highlighting the importance of early intervention. We determined the minimum effective dose and the associated pharmacokinetic (PK) and exposure relationship of RG3039 and DcpS inhibition *ex vivo*. These data support the long PK half-life with extended pharmacodynamic outcome of RG3039 in 2B/− SMA mice. In motor neurons, RG3039 significantly increased both the average number of cells with gems and average number of gems per cell, which is used as an indirect measure of SMN levels. These studies contribute to dose selection and exposure estimates for the first studies with RG3039 in human subjects.

INTRODUCTION

Proximal spinal muscular atrophy (SMA) is an autosomal recessive neuromuscular disease characterized by symmetric proximal muscle weakness that is secondary to the loss of α-motor neurons in the spinal cord (1). It is one of the leading hereditary causes of infant and early childhood mortality, with an estimated incidence of 1 in 8–10 000 in populations of Eurasian ancestry (2,3). SMA is clinically heterogeneous with age of onset from infancy to adulthood. To facilitate clinical stratification, SMA is divided into four major types (I–IV) based on age at onset and highest achieved motor milestones; with Type I representing the most severe patients and Type IV representing the mildest patients (4–6). SMA is caused by insufficient levels of the survival motor neuron (SMN) protein. The majority of patients (>94%) have a homozygous deletion/mutation in the *survival motor neuron 1*

*To whom correspondence should be addressed at: Lurie Children's Research Center, 2430 N Halsted St. Chicago, IL 60614, USA. Tel: +1 7737556352; Fax: +1 7737556345; Email: c-didonato@northwestern.edu
†These authors contributed equally to this study.

(SMN1) gene at 5q13 (7,8). Humans possess a nearly identical paralog, *SMN2,* which is adjacent to *SMN1,* and at least a single functional copy is present in all SMA patients. The principal difference between the two *SMN* genes is a translationally silent, single nucleotide transition in *SMN2* exon 7 that promotes exon skipping during RNA processing (9,10). This results in a truncated, dysfunctional protein that is rapidly degraded (11). Consequently, the small amount of functional protein produced from *SMN2* cannot fully compensate for loss of *SMN1*. However, *SMN2* shows copy number variation and this enables it to modify SMA into the various clinical subtypes (3,12). Family studies and mouse models show that increased *SMN2* copy number correlates with a milder disease course (3,7,12–14).

The goal of early SMA drug discovery programs has been to identify small molecules that induce SMN from *SMN2*, a ubiquitous gene target in the SMA population (15–19) [additionally reviewed in (20,21)]. An example is the C5-substituted 2,4-diaminoquinazolines. This class of compounds was originally identified using a human *SMN2* promoter cell-based reporter assay (15). A focused medicinal chemistry effort led to the generation of approximately one thousand 2,4-diaminoquinazoline analogs (22). The lead compounds from this effort are highly potent in the cell-based *SMN2* promoter assay and can induce an increase in nuclear gem/Cajal body numbers (22). Gem loss is a cellular hallmark of fibroblasts derived from SMA patients and their numbers inversely correlate with disease severity. One protein target of C5-substituted quinazoline compounds is DcpS (23), a nuclear shuttling protein that binds and hydrolyzes the m7GpppN mRNA cap structure and is a modulator of RNA metabolism (24–26). Co-crystallization studies indicate that upon binding, C5-substituted 2,4-diaminoquinazolines hold the DcpS enzyme in a catalytically incompetent conformation (23). The potency of inhibition of DcpS decapping activity by these compounds *in vitro* correlates with their potency for *SMN2* promoter induction in a cell-based assay across a 1000-fold range in activity (23). However, despite this strong correlation, the mechanism by which DcpS inhibition elevates SMN expression remains unknown. To gain insight into efficacy, the C5-substituted 2,4-diaminoquinazoline, D156844, was tested in delta-7 SMA mice, a severe mouse model of SMA. Oral administration of this earlier lead quinazoline analog, increased the mean lifespan of delta-7 SMA mice and ameliorated motor phenotypes (27,28). These data provided the basis for further medicinal chemistry optimization that culminated in the identification of D157495, also known as RG3039, as the clinical development candidate.

The goal of the work described here was to elucidate RG3039's effect on disease pathology, in particular the motor neuron circuit, in SMA mice of varying disease severity. In the work described herein, we have used measures of efficacy and pathological improvement to determine the minimum effective dose (MED) in SMA mice and evaluate the pharmacokinetic (PK) and pharmacodynamic (PD) properties of RG3039.

RESULTS

In vivo exposure analysis of RG3039 in adult and neonatal mice

RG3039 displays a potent DcpS inhibitor activity with an IC_{50} of 4.2 ± 0.13 nM and an IC_{90} of 40 nM (Fig. 1A and B) using the previously described DcpS inhibition assay (23). To assess oral bioavailability and central nervous system penetration, a full PK profile for RG3039 was determined in adult mice (eight time points, $n = 5$/time point) following a single 10 mg/kg po (gavage) administration in 0.5% hydroxypropylmethylcellulose (HPMC) − 0.1% Tween 80 in water. Table 1 summarizes the PK parameters and Supplementary Material, Figure S1 shows the levels of RG3039 in plasma and brain versus time. These data show good brain penetration with high brain-to-plasma partitioning and a half-life of ∼10 h. Evaluation of tolerability and relative exposure was performed following a repeat dose escalation study using wild-type (WT) mouse pups. For these studies, RG3039 was administered in water po, once per day (qd) to pups starting on postnatal (P) Day 5, for up to 8 days with doses from 15 up to 45 mg/kg. Plasma and brain samples were taken 1 h post-dose on the last day of the study. Table 2 summarizes the dose-dependent exposure data for RG3039 in WT neonatal mice. The brain exposure for pups was higher than anticipated based on the single-dose PK in adult mice, however, this is likely attributable to the immature blood–brain barrier in neonates and/or drug accumulation over 8 days of dosing. The accumulation is supported by comparing brain levels following single versus repeat dosing for 45 mg/kg (Groups 3 and 4, Table 2). Importantly, for each dosing paradigm, all pups appeared normal, had good ambulation, showed weight gain similar to the vehicle-treated (water) group and tolerated the high drug exposure during the short treatment period (data not shown). Based on these collated results that included exposure data in mice, weight gain and overall tolerability with up to eight consecutive days of oral dosing in WT neonatal mice (of up to 45 mg/kg), an initial dose of 20 mg/kg was selected for efficacy studies in SMA model mice as described below.

RG3039 increases lifespan and improves function in the Taiwanese SMA mouse model

To gain insight into the therapeutic potential of RG3039, we performed blinded studies using two SMA mouse models. Further details of breeding, handling and study execution are detailed in the Materials and Methods section. For the first study Taiwanese hemizygous SMA mice, $(SMN2)2Hung^{tg/0};Smn^{tm1Hung/tm1Hung}$, here termed 5058 Hemi SMA mice, were used. This model was generated and described by Li and coworkers (14), and has a similar survival timeframe as delta-7 SMA mice (28). Since our original re-characterization of this line (29), the phenotypic and survival variability has been reduced through backcrossing to FVB/N mice. The maximum survival of untreated 5058 Hemi SMA mice is now 12 days, with an average and median survival of 9 and 10 days, respectively, and clear symptom manifestations starting at P4 (data not shown). This is consistent with reports from other investigators using this model in an FVB/N background for preclinical studies (30–32). Starting at P4, mice were treated qd by oral gavage with RG3039 (20 mg/kg) or vehicle (water). The mice were followed for survival, weight and righting reflex (Supplementary Material, Fig. S2). It is important to note that the survival and righting reflex results lead to successfully unblinding this study. RG3039-treated SMA mice ($n = 20$) had a median survival that was 38% greater than vehicle-treated SMA mice ($n = 19$) (Supplementary Material, Fig. S2A; $\chi^2 = 9.210$,

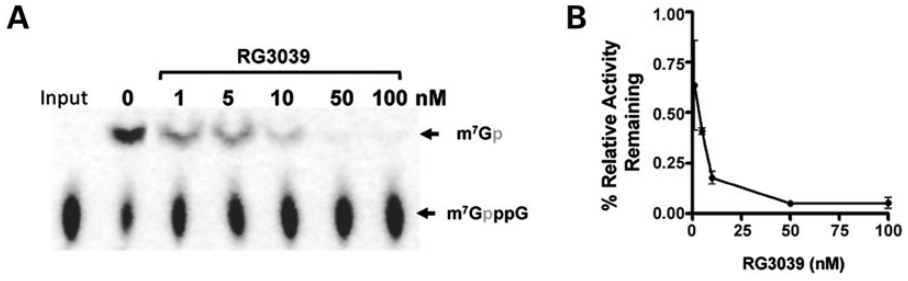

Figure 1. RG3039 inhibits the decapping enzyme DcpS. (**A**) RG3039 inhibits hDcpS enzyme activity in a dose-dependent manner *in vitro* ($n = 3$ experimental replicates) and is graphically shown in (**B**). The IC_{50} is 4.2 ± 0.13 nM and IC_{90} is 40 nM.

$P = 0.0024$). Furthermore, when placed on their back, RG3039-treated SMA mice were able to right within ∼10–14 s until P11. This differentiated RG3039-treated 5058 Hemi SMA mice from vehicle-treated SMA mice where the later progressed from ∼13 ± 3 s at P6 to 41 ± 13 s at P10 (Supplementary Material, Fig. S2C). Therefore, these collective results suggest that RG3039 is able to slow disease progression in 5058 Hemi SMA mice even when the drug is administered well after symptoms have emerged.

RG3039 increases lifespan and improves function in the 2B/− SMA mouse model

For our second set of efficacy studies, we used the 2B/− SMA mouse developed in the Kothary and DiDonato laboratories (33,34). The 2B/− SMA mouse is an alteration of the murine *Smn* locus (33,34) and although the model does not contain *SMN2*, we knew from prior work that the C5-substituted 2,4-diaminoquinazoline compounds induce *Smn* expression from the endogenous mouse gene (22,27). When the 2B allele is combined with the *Smn* null allele in an FVB/N background ($Smn^{+/-}$) (35), the resulting SMA mice (2B/−) have a consistent survival rate and slower disease progression than either 5058 Hemi SMA mice or delta-7 SMA mice that are also in an FVB/N background. Starting at P4, an early point in disease course prior to motor neuron loss, neuromuscular manifestations or obvious non-neuromuscular phenotypes, 2B/− SMA mice and sibling controls (2B/+) were dosed po qd with RG3039 (20 mg/kg) or vehicle (water) until death or P20 and followed until the study endpoint at P120. Mice were monitored for survival, weight and functional parameters that included righting reflex, heart rate, gait and inclined planes. A cohort of untreated 2B/− SMA mice ($n = 15$) were followed at the same time in this study and their median survival was 21 days, with a maximum lifespan of 25 days (data not shown). Treatment with vehicle had no detrimental effect on the survival of control pups ($n = 19$), but significantly reduced the median and maximal survival of 2B/− SMA mice ($n = 18$) to 18.5 and 21 days, respectively (Fig. 2A; $\chi^2 = 3.937, P < 0.05$) and is likely attributable to the stress of daily po dosing (Fig. 2A). In stark contrast to the vehicle-treated SMA mice, RG3039 treatment extended survival in 100% of the treated 2B/− SMA pups ($n = 22$), to at least P26. We ended the study at 120 days. At that time 27% (6/22) of the RG3039-treated 2B/− SMA mice were still alive. The median survival of this cohort was 112 days, more than a 600% increase in survival over vehicle-treated 2B/− SMA pups (Fig. 2A).

The body mass of both SMA treatment groups differed from control mice by P12 but remained similar to each other until both reached their peak, pre-weaning weight at P15. Thereafter, both SMA groups lost weight, but RG3039 treatment tempered the rate of loss in SMA mice and by P23–P27 they began to gain weight (Fig. 2B). During this same period, we monitored general function, grooming and heart rate. While all dosing was performed blinded, at P16 we were clearly able to unblind the RG3039-treated SMA mice from vehicle-treated SMA mice using these parameters in our first several litters of treated mice (Fig. 2C).

We have previously used heart rate to monitor overall health in neonatal SMA mice and their disease progression (36,37). At P16, the heart rate of vehicle-treated 2B/− SMA mice ($n = 10$) is ∼18% slower than that of control siblings ($n = 7$) and it continues to slow as the disease progresses. RG3039 treatment ($n = 9$) improved 2B/− SMA mouse heart rate by 11% (727 ± 12 versus 652 ± 15 bpm, $P = 0.001$), and this lessened the significant difference we observed between 2B/− SMA and control mice ($n = 6$). Importantly, there was no difference in the heart rate of control mice treated with RG3039 or vehicle (761 ± 12 versus 770 ± 10 bpm, $P = 0.391$).

Although early drug treatment provided a clear survival and functional benefit when compared with vehicle-treated mice, RG3039-treated SMA mice were smaller than their RG3039-treated 2B/+ control sibling littermates from P12 onwards (Fig. 2B). At weaning, a very mild tremor was noted, which became more pronounced with age. RG3039-treated SMA mice had good ambulatory function, which further improved when the mice began to gain weight again after P25. Thereafter, their weight gain paralleled that of control mice until ∼P105 (15.1 ± 0.3 g SMA versus 27.4 ± 3.6 g control), with a slight decrease by the study endpoint at P120. Overall, RG3039-treated 2B/− SMA mice could rear, grasp and ambulate, although to a lesser degree when compared with controls (Supplementary Material, Video S1). The median survival was 112 days even though drug treatment ended on P20. We applied treadmill walking on a transparent belt with ventral plane videography (DigiGait, Mouse Specifics, Inc., Boston, MA, USA) to determine indices of gait, gait variability and the maximum ambulatory speed of RG3039-treated mice over time. For example, at P60 ($n = 16$), the average, median and maximum ambulatory speed was 6.9 ± 1.1, 6.0 and 13.0 cm/s, respectively. As a reference, vehicle- and RG3039-treated 2B/+ control mice easily ambulate at speeds >21 cm/s. Over time, the hind limbs were more affected than the forelimbs, but

Table 1. PK parameters[a] for RG3039 single dose adult (WT) mouse PK (po) at 10 mg/kg (8.5 mg/kg, free base form)

	Dose (mg/kg)	C_{max} (ng/ml)	C_{max} (μM)	AUC_{last} (ng.h/ml)	$AUC_{0\text{-}inf}$ (ng.h/ml)	CL_F (ml/h/kg)	T_{max} (h)	Half-life (h)
Plasma	10 (8.5)	25.6	0.06	156.8	285.8	35 153	0.5	10.6
Brain	10 (8.5)	418	0.97	6762	7049	1428	6.0	9.62

[a]The time versus concentration profile data for $n = 5$ adult mice per time point is shown in Supplementary Material, Figure S1. The mean exposure values were used for calculations of PK parameters.

they were still able to aid in locomotion and balance. Those mice that survived to the study endpoint (P120) had righting reflex times between 1 and 3 s. As an additional test of motor ability, muscle strength and coordination, we used 35 and 55° inclined planes. We developed this test for the milder 2B/− SMA mice, as a simple, non-invasive way of measuring overall body strength and coordination. Mice were placed face down on 35 and 55° inclined planes and monitored for their ability to turn from a face-down position to a face-up position and climb to the top of the incline. This requires flexor, extensor, proximal, distal and core muscles to successfully complete the task. At the study endpoint, 67% (4/6) were able to do this on the 55° incline and 83% on a less steep 35° incline (Supplementary Material, Video S2).

Therapeutic window of RG3039

To investigate RG3039's therapeutic window for responsiveness in 2B/− SMA mice, we delayed drug administration until P11 ($n = 13$). We chose P11 as this is 1 day before weight begins to differentiate SMA mice from controls and symptoms begin to be manifested (i.e. elevated liver enzymes and motor neuron deficits). The impressive benefit that we obtained with early drug delivery was absent when delaying treatment to P11. The median survival was 23 days and although statistically significant, the survival benefit was only minimally improved over vehicle-treated SMA mice (Fig. 2A; $\chi^2 = 14.84$, $P < 0.0001$). Hence, the therapeutic window for RG3039 in this SMA mouse model is nearly closed by P11. The comparison of pairwise survival between P4 versus P11 drug delivery in 2B/− SMA mice was significant ($P < 0.0001$) and demonstrates the superior outcome of RG3039 when delivered early in disease rather than late.

Dose-dependent survival and function of RG3039 in 2B/− SMA mice define the MED

To determine RG3039's MED in 2B/− SMA mice, the efficacy study at 20 mg/kg was used as a baseline. SMA mice were dosed po, qd from P4 to P20 with varying doses of drug ranging from 0.25 to 10 mg/kg. The median lifespans of RG3039-treated SMA mice were 20 days (0.25 mg/kg, $n = 18$), 22 days (0.5 mg/kg, $n = 11$), 123 days (2.5 mg/kg, $n = 24$), 134 days (10 mg/kg, $n = 9$) and 112 days (20 mg/kg, $n = 22$) compared with 18.5 days for vehicle-treated and 20 days for untreated 2B/− SMA mice ($n = 21$) (Fig. 3A). The survival advantage was significant for all groups (log rank, $P < 0.001$) except the lowest dose, 0.25 mg/kg. Although the 0.5 mg/kg cohort had improved survival when compared with vehicle or untreated mice (5 and 2 days, respectively), it was negligible and significantly less than the 2.5, 10 and 20 mg/kg cohorts (log rank, $P < 0.001$). The survival curves of the 2.5 and 10 mg/kg cohorts were similar to the 20 mg/kg cohort. The median survival timeframes of these groups (123 days for 2.5 mg/kg and 134 days for 10 mg/kg) were slightly longer than the 112 days of the 20 mg/kg cohort, but not statistically different (log rank, $P = 0.9338$). The body mass and rate of gain for all treatment groups was unremarkable pre-weaning, and all had the same weight drop from P15 to P25. Post-weaning, the slope of weight gain was comparable until P90 (Fig. 3B).

Over the course of this study, several well-functioning mice died unexpectedly (such as first and last mice in Supplementary Material, Video S1). There were no signs of distress, such as weight loss, decreased activity or reduced grooming. In five other instances, regardless of their mobility as good, intermediate or poor, mice became severely ill over the course of 1–2 days and required euthanasia (two at 2.5 mg/kg, one at 10 mg/kg and two at 20 mg/kg). Upon necropsy, they had enlarged kidneys and engorged bladders from urinary retention. Similar issues of bladder retention, priapism and bowel obstruction were recently noted in delta-7 SMA mice that received a morpholino antisense oligo and had extended survival (38). These symptoms are possible signs of autonomic nervous system dysfunction, which we have previously reported in severe inducible and delta-7 SMA mice with others (36,37,39). Similar to that report, the mice in this study were also acutely affected.

Treadmill walking, gait dynamics and inclined planes were used to quantify function at regular intervals. At P30, the three surviving RG3039-treated SMA cohorts (2.5, 10 and 20 mg/kg) were very similar in function for both inclined planes and gait (Fig. 3C–G and data not shown). By 6–9 weeks of age-treated cohorts began to differentiate based on function. The 2.5 mg/kg cohort was inferior on the inclined planes and had a 70% pass rate at 35° versus 31% pass at 55° (Fig. 3C). The median of the maximum ambulatory speed for both the 2.5 and 10 mg/kg cohorts at P60 was 3.0 versus 6.0 cm/s for the 20 mg/kg dose, which was not significantly different (Fig. 3D). The small sample size of the 10 mg/kg group may not represent the maximum walking speed of this group. Gait dynamics of mice walking at 10 cm/s at P60 were evaluated and the temporal and spatial indices of gait for both the fore- and hind-paws from the 2.5 and 20 mg/kg cohorts (Fig. 3E–G) were compared. Although the mice were the same size, the stride length was significantly different (Fig. 3F). To account for the differences in stride length, the 2.5 mg/kg cohort had a higher step frequency (data not shown) along with multiple other variations in their gait pattern. Figure 3G illustrates some of the significant temporal indices for the hind limbs. Collectively, on the basis of survival and functional data we determined the MED for RG3039 to be 2.5 mg/kg.

Table 2. Drug exposure of RG3039 after repeat dosing to WT neonates starting at 5 days of age

Group	Dose[a] (mg/kg) (qd, po)	Dosing period (days)	Plasma levels (ng/ml)	Brain levels (ng/g)	Plasma levels (mM)	Brain levels (μmole/kg)	Relative ratio (single versus repeat dosing) Plasma	Brain
1	15 (12.8)	8	167	3363	0.39	7.78		
2	30 (25.6)	8	236	20 821	0.55	48.20		
3	45 (38.5)	8	271	32 589	0.63	75.44	1.31	7.11
4	45 (38.5)	1	207	4581	0.48	10.60	1.0	1.0

[a](Dose as free base form) Groups 1, 2 and 3 ($n = 8$), Group 4 ($n = 5$) neonates. Average values shown.

PK and exposure relationship of target engagement for RG3039 in SMA mice

RG3039 is a potent inhibitor of DcpS (the scavenger decapping enzyme), which is known to modulate RNA metabolism (23). We investigated the PK/PD relationship by correlating RG3039 brain levels with the extent and duration of DcpS inhibition *ex vivo*. The brain tissues and plasma were collected at various time points following the last day (P20) of P4–P20 qd, po dosing with RG3039 at 20 and 2.5 mg/kg. RG3039 PK parameters are shown in Table 3 for 2.5 and 20 mg/kg dose groups. Similar to the PK analysis in WT mouse pups (Table 2), high brain exposure (brain/plasma ratio) was observed in 2B/− SMA mice (Table 3). With the RG3039 elimination half-life from brain tissues of 40 and 31 h for 20 and 2.5 mg/kg dose, respectively, brain accumulation is expected. Brain accumulation was observed at 20 mg/kg (as seen by the larger brain-to-plasma ratio at 20 than 2.5 mg/kg as measured by AUC ratio: 31 at 20 mg/kg and 9.3 at 2.5 mg/kg; and by C_{max} ratio: 16 at 20 mg/kg and 9.3 at 2.5 mg/kg).

To assess DcpS activity, the brain tissues from RG3039-treated 2B/− SMA mice at various time points following the last day (P20) of oral dosing at 20 and 2.5 mg/kg were collected and homogenized. The homogenates were used for determination of the DcpS decapping activity using the radiolabeled m7Gp*ppG substrate following our previously described protocol (23). As shown in Figure 4A, the DcpS activity at the 20 mg/kg for the P4–P20 dosing regimen was fully inhibited in brain samples from mice at 120 h (5 days) post-last dose. In contrast, treating SMA mice at this same dose (20 mg/kg) with a single administration on P11 indicates ∼5% residual DcpS activity (i.e. 95% DcpS inhibition) at 72 h post-dose, but by 168 h (7 days) residual DcpS activity in the brain homogenates increased to ∼10% (i.e. ∼90% enzyme inhibition) (Fig. 4B). The 72 h DcpS inhibition data for all three dose groups (Fig. 4A–C) clearly paralleled the RG3039 levels in brain homogenates at the 72 h time point (Supplementary Material, Fig. S3). This is further substantiated when we evaluated the DcpS activity from brain homogenate samples from 2.5 mg/kg (MED) cohorts; the results showed increasing DcpS activity with time, as is evident from the bar graph data shown in Figure 4C. These data indicate that the increase in DcpS activity with time post-dosing from the 2.5 mg/kg dosed animals, and nearly complete inhibition of DcpS activity from the 20 mg/kg animal brain samples for an extended period of time are consistent with the long PK and PD half-life in the target tissues.

RG3039 increases gem number in SMA spinal motor neurons

It has previously been demonstrated that the inhibition of DcpS activity can modulate SMN *in vitro* and increase SMN gem numbers in patient-derived primary fibroblasts (15,22). Gems, or Gemini of Cajal bodies are SMN containing nuclear structures whose numbers correlate with SMN levels within the cell (13,40). They have been used as a measure of SMN protein levels within the nucleus and a screening tool in high throughput drug discovery programs (15,16,18,41). To ascertain the effects of RG3039 treatment on Smn protein and gem numbers in SMA mice, 2B/− mice were treated from P4 to P16 with either vehicle or RG3039 (20 mg/kg) and tissues were harvested at 2, 4 and 20 h post-last dose (P16) ($n = 3–6$/time point). Interestingly, there was no significant difference in total Smn protein levels in brain, spinal cord, skeletal muscle or kidney compared with vehicle-treated SMA mice (Supplementary Material, Fig. S4).

We further assessed RG3039's ability to increase Smn levels specifically within the nuclear compartment by counting gems within motor neurons. Spinal cords from control and SMA mice treated with either vehicle or RG3039 were harvested (P16) and immunostained for choline acetyltransferase (ChAT) to identify motor neurons and Smn to identify gem structures (Fig. 5A). Gems were counted independently by two individuals in a blinded fashion with very similar results. Consistent with human SMA patient fibroblasts data and gem numbers in motor neurons from other SMA mouse models, only ∼20% of the motor neurons from 2B/− SMA mice contain gems ($P \leq 0.001$ compared with 2B/+ controls). However, RG3039 treatment doubled the number of motor neurons containing gems and increased the average number of gems/motor neurons. This increase in gem number with RG3039 treatment restored the number of motor neurons that contained gems to ∼75% of control motor neurons (Fig. 5B). These data indicate that RG3039 modestly increases total Smn levels in many tissues, but in motor neurons, the primary target cell type of SMA treatment strategies, Smn, is being increased/redistributed to the nuclear compartment.

RG3039 tempers motor unit pathology and dysfunction

SMA is characterized by motor neuron loss and consequent muscle atrophy. These same features have been well established in SMA mice along with defects in the maturation and function of peripheral synapses (28,42–45). To gain insight into RG3039's

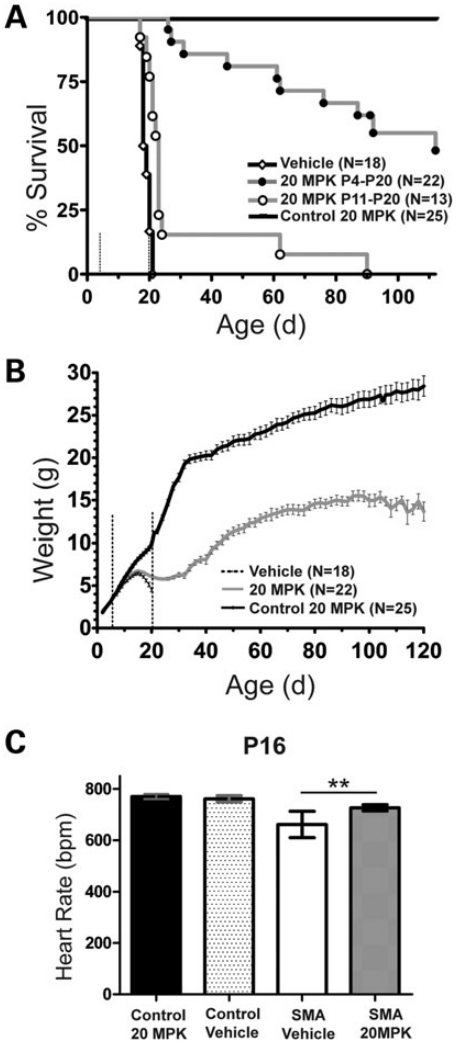

Figure 2. Oral delivery of RG3039 increases survival, weight and heart rate in 2B/− SMA mice. (**A**) The Kaplan–Meier survival curve comparing RG3039 control (2B/+, $n = 25$), vehicle 2B/− SMA ($n = 18$) and RG3039 2B/− SMA ($n = 22$) all dosed P4–P20; also included is P11–P20 RG3039 2B/− SMA ($n = 13$). RG3039 was dosed at 20 mg/kg (MPK). The median survival for each group, 20 MPK P4–P20 (112 days) and 20 MPK P11–P20 (23 days), was significant when compared with vehicle-treated 2B/− SMA mice (18.5 days), log-rank test, $P < 0.0001$. The median survival of pairwise comparison between P4–P20 and P11–P20 SMA RG3039-treated mice was significantly different, by log-rank test, $P < 0.0001$. Dashed lines in panels (A) and (**B**) represent the treatment window, P4–P20. (B) Weight curves from P2 to P120 of RG3039-treated control (black), P4–P20 2B/− SMA vehicle (dashed) and P4–P120 RG3039-treated 2B/− SMA mice (20 MPK) (gray). Note the max weight achieved in both SMA treatment groups is P15 with a subsequent decline. After P25, RG3039-treated 2B/− SMA mice parallel the weight gain seen in control mice until ∼P105. Weight is shown as the average ± SEM. (**C**) Heart rates from ECG recording at P16 were obtained from conscious mice and used to assist in unblinding the drug study. Control 20 MPK ($n = 6$), control vehicle ($n = 7$), SMA 20 MPK ($n = 9$) and SMA vehicle ($n = 10$). Heart rate is shown as the average ± SEM. $^{*}P < 0.05$, $^{**}P < 0.01$, Student's *t*-test.

ability to preserve or enhance motor unit function, we first analyzed motor neuron number from blinded cryosections of lumbar spinal cord segments L2–L5 from P4 to P16 vehicle and RG3039-treated 2B/− SMA mice. After unblinding, it was determined that SMA pups receiving vehicle treatment had ∼27% fewer motor neurons than control mice. RG3039 treatment attenuated this loss, so that the number of motor neurons did not differ significantly from controls (Fig. 6A), but this trend of improvement did not reach statistical significance when comparing vehicle with RG3039-treated SMA mice (11.8 ± 0.0 and 14.7 ± 0.6; Fig. 6A).

To further explore this trend of motor neuron protection, motor neuron counts were separated into their respective motor pools as recent data have shown that motor neurons in the medial motor column (MMC) are preferentially affected in delta-7 and severe inducible SMA mice (36,46). Analogous to those reports, MMC motor neurons are significantly reduced in vehicle-treated 2B/− SMA mice (42.7 ± 3.8%, $P \leq 0.01$) when compared with controls, and importantly, RG3039 treatment significantly improves this (33.8 ± 3.2%, $P \leq 0.05$) (Fig. 6B). The lateral motor column (LMC) also had a significant loss of motor neurons (34.7 ± 0.7%, $P \leq 0.05$), which was slightly reduced with RG3039 treatment (Fig. 6C). Since there are more motor neurons in the LMC region, it explains the trend toward improvement in total motor neurons. Thus, RG3039 treatment improves motor neuron number irrespective of spinal column location.

To assess the peripheral neuromuscular junctions (NMJs), we examined the pre- and post-synaptic architecture in the intercostal (IC) and triangularis sterni (TS) muscles (Fig. 7A) ($n = 5$/group). These muscles were chosen due to their role in maintaining proper breathing function, one of the most critical deficits that afflict SMA patients. At P18, a significant number of NMJs in both the ICs and TSs of vehicle-treated 2B/− SMA mice were no longer fully innervated and had a corresponding increase in partially innervated junctions (Fig. 7B and D, $P < 0.001$). RG3039 treatment significantly improved fully innervated ICs with the associated decrease in partial innervation ($P = 0.005$), but interestingly, there was no improvement in fully or partially innervated TS NMJs.

A hallmark of pre-synaptic neurodegeneration that has been reported in other SMA models is axonal swellings marked by neurofilament accumulation (36,42,43,45). Approximately 15% of both vehicle- and RG3039-treated 2B/− SMA mice had axonal swellings, suggesting that RG3039 had no effect on the underlying cause of these neurofilament aggregates. We also examined whether axonal sprouting/failed pruning of NMJs was occurring with RG3039 treatment. There was no evidence to support this in the IC muscle, but in the TS, this occurred in 12% of the NMJs analyzed. This was statistically significant ($P < 0.05$) when compared with control TS muscle, but when compared with vehicle-treated mice that had 5% sprouting, the positive trend did not reach statistical significance (Fig. 7C and E).

The post-synaptic motor endplate maturity in SMA mice was also analyzed following RG3039 treatment. We observed that motor endplates in the IC and TS of vehicle and RG3039-treated 2B/− SMA mice were significantly less mature and both had significantly increased numbers of folds relative to control littermates (Fig. 7F–H). However, RG3039 treatment attenuated this phenotype, and for the TS, significantly increased the number of motor endplates with secondary structure relative to vehicle-treated 2B/− SMA mice ($P \leq 0.05$) (Fig. 7G and H).

To complement the histologic findings, neurophysiologic studies on P18 mice similarly treated as above were performed to functionally assess the motor unit. Compound muscle action

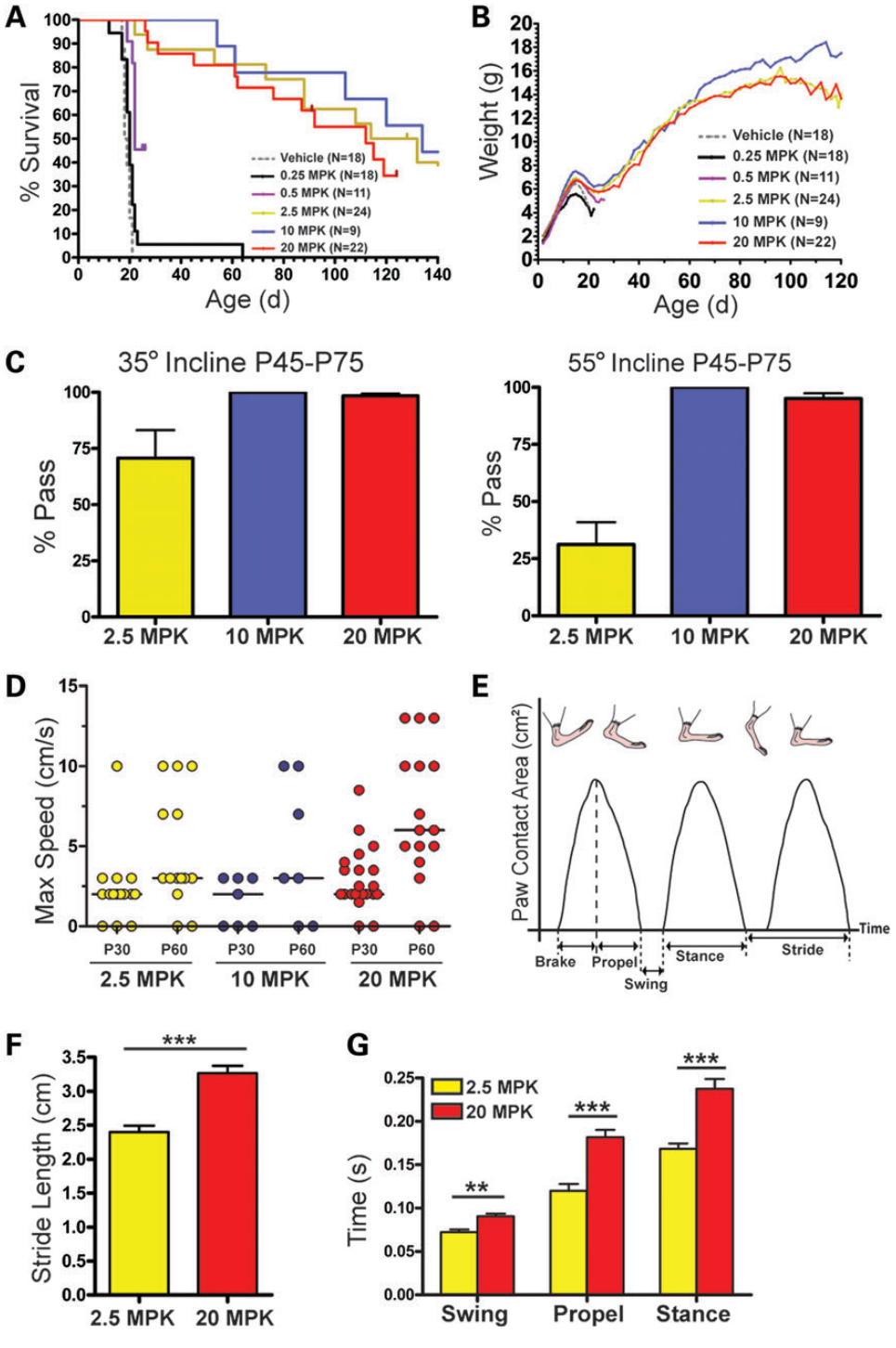

Figure 3. RG3039 treatment improves survival and function of 2B/− SMA mice in a dose-dependent manner. (**A**) Kaplan–Meier survival curves of 2B/− SMA pups treated with varying doses (0.25–20 mg/kg) (po) daily from P4 to P20 and followed for survival and function. The median survival of drug-treated mice with a significant survival benefit compared with vehicle-treated SMA mice was 22–134 days [0.5 mg/kg ($n = 11$), 2.5 mg/kg ($n = 24$), 10 mg/kg ($n = 9$) and 20 mg/kg ($n = 22$), by log-rank test, $P < 0.0001$]. The lowest dose 0.25 mg/kg ($n = 18$) did not differ significantly from vehicle-treated SMA mice ($n = 18$). (**B**) Body weight graphs (average ± SEM) of the mice shown in (A). (**C**–**G**) Functional assays post-weaning across the surviving treatment cohorts of inclined planes (C) and gait dynamics (D–G). (D) The maximum ambulatory speed (cm/s) of each RG3039-treated 2B/− SMA mouse alive at that time point. (E) Schematic representation of the basic components of stride as a function of paw contact area. (F) P60 stride length at 10 cm/s and (G) examples of hind-limb gait differences at 10 cm/s. The *P*-values between different treatment cohorts (C and D) were determined by one-way ANOVA and Bonferroni multiple post hoc comparisons. Statistical comparisons in (F) were done by Student's *t*-test with normally distributed data comparing P60 SMA mice at 10 cm/s that had been previously dosed at 2.5 and 20 mg/kg. $^{*}P \leq 0.05$, $^{**}P \leq 0.01$, $^{***}P \leq 0.001$.

Table 3. RG3039 2B/− SMA mouse PK at 20 and 2.5 mg/kg (MPK) (17 and 2.0 mg/kg free base form, respectively)

	Dose (mg/kg)	C_{max} (ng/ml) (ng/g)[a]	AUC_{last} (ng.h/ml) (ng.h/g)[b]	T_{max} (h)	Half-life (h)	Relative ratio brain/plasma AUC (C_{max})	Ratio 20–2.5 MPK AUC (C_{max})
20 MPK							
Plasma	20	205	6380	2	20		10 (7)
Brain	20	3300[a]	200 000[b]	2	40	31 (16)	34 (12)
2.5 MPK							
Plasma	2.5	28.7	634	2	13[c]		
Brain	2.5	267[a]	5880[b]	2	31	9.3 (9.3)	

[a]ng/g.
[b]ng.h/g.
[c]Five-day point excluded (one animal >LLOQ; lower limit of quantification).

potential (CMAP) amplitudes were recorded from the sciatic innervated gastrocnemius muscle after nerve stimulation at the sciatic notch, along with repetitive nerve stimulation (RNS) to assess functional NMJ integrity. Both vehicle- and RG3039-treated SMA mice had reduced CMAP amplitudes indicating axonal loss. Their amplitudes were not significantly different from each other or untreated SMA 2B/− mice, but decreased when compared with controls ($P < 0.001$, Fig. 7I and data not shown). These results were consistent with the total and LMC motor neuron counts. The RNS studies to assess NMJ integrity were revealing. As background, healthy NMJs should demonstrate no decrement to RNS; however, to allow for technical factors, decrements >10% are considered clinically significant in clinical EMG. Control mice showed no decrement with 3 or 10 Hz stimulation ($n = 4$, range 0–8%, mean $3.3 \pm 1.7\%$). However, as shown in Figure 7J, decrements in CMAP amplitudes after 3 Hz stimulation in untreated or vehicle-treated SMA mice ($n = 6$) ranged from 12 to 32% and averaged $19.8 \pm 2.7\%$. Percent decrement was greater at higher rates of stimulation (10 Hz; range 19–34%). In contrast, RG3039 treatment seemed to enhance neuromuscular transmission in 2B/− SMA mice ($n = 5$), as the decrement at 3 Hz was mitigated to 9–18% with an average of $12.6 \pm 1.5\%$ (Fig. 7J), an increase of ∼37% when compared with vehicle-treated mice ($P = 0.04$). These physiologic findings of enhanced neuromuscular transmission are in agreement with the increased innervation and NMJ maturity demonstrated histologically in different muscle groups.

The motor neuron and NMJ defects within SMA mice and patients result in muscle atrophy. To gain insight into the molecular changes that occur within the skeletal muscle of 2B/− SMA mice compared with control mice, a polymerase chain reaction (PCR) screening array was used to simultaneously profile the expression of 84 genes involved in skeletal muscle atrophy and regeneration. As shown in the volcano plot in Figure 8A, 12 genes were either up- or down-regulated >2.0-fold and statistically significant when comparing vehicle-treated 2B/− SMA mice with vehicle-treated 2B/+ control mice, and may represent biomarkers for this SMA mouse model. This analysis was also done with RG3039-treated 2B/− SMA mice. Some interesting observations were noted when comparing the volcano plots of vehicle- or RG3039-treated 2B/− SMA mice with control mice (Fig. 8A and B). There was a general trend of differentially expressed genes in vehicle-treated 2B/− SMA mice (Fig. 8A) to move back toward the vertical baseline of 0-fold change with RG3039 treatment in 2B/− SMA mice (see orange lines, Fig. 8B), implying an improvement. A noted significance was observed in the transcript level of IGF-1, which was 1.62-fold higher in a *direct* comparison of vehicle and RG3039-treated SMA skeletal muscle ($P = 0.012$) (Fig. 8 and Supplementary Material, Fig. S5). IGF-1 dysregulation in SMA mice and subsequent correction with *SMN2* exon 7 splice-switching ASOs has also been reported in another model of SMA (31). Overall, these transcriptional profiling results suggest that disease consequences in skeletal muscle may be less severe in RG3039-treated 2B/− SMA mice than vehicle-treated 2B/− SMA mice. This is consistent with the observation of overall improvement of NMJ morphology and neurophysiology in RG3039-treated 2B/− SMA mice.

DISCUSSION

Here, we report the pharmacological characterization of the orally active quinazoline derivative RG3039. We demonstrate that RG3039 is able to extend survival and improve function in two SMA mouse models of differing severity and we show that RG3039 can positively impact neuromuscular pathologies. Our work evaluated effects of dose variation on survival and functional measures, PK in 2B/− SMA mice and drug brain exposure versus target (DcpS) inhibition.

Using genetic, biologic or small molecule approaches, multiple studies have now shown that early intervention can have a profound impact on survival and phenotype in SMA model mice (27,31,47–53). Consistent with these studies, we found that RG3039 treatment had a substantial survival benefit in 2B/− SMA mice of >600% (P112–P134 for RG3039 versus P18 for vehicle) when dosing started at P4, an early point in disease. Delaying administration of drug until P11, after clear symptom onset in this model, essentially mitigated the positive response. Dosing in the more severe 5058 Hemi SMA pups following symptom onset (P4) also confirmed this result in a second SMA model. This highlights two key points: (i) early intervention is key to providing the best outcome with whatever treatment modality is used and (ii) early diagnosis of SMA infants through newborn screening may have the potential to significantly improve therapeutic benefit of treatment.

The ability to identify RG3039-treated SMA cohorts in blinded mouse studies demonstrates this drug can be beneficial after symptoms are manifested. In further support of

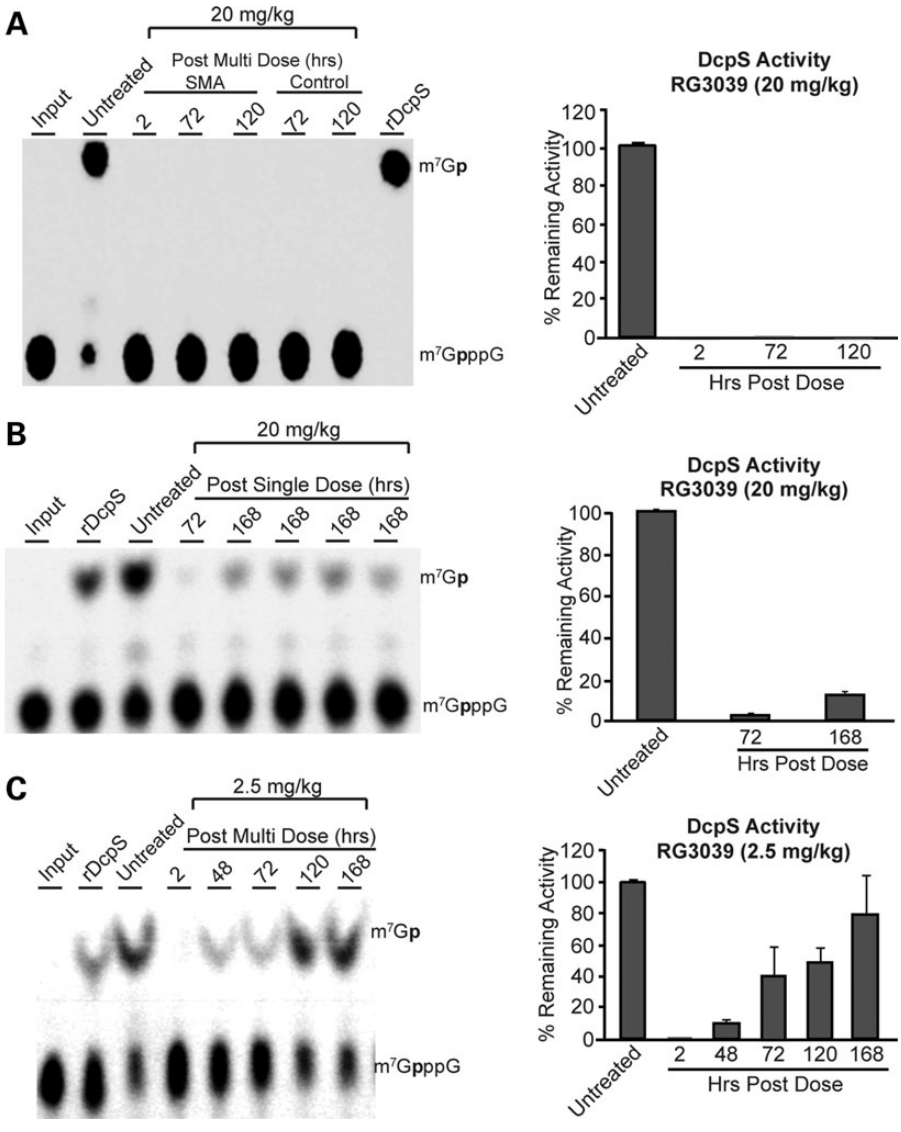

Figure 4. RG3039 inhibits DcpS activity. The inhibition of DcpS decapping activity in brain homogenates following po dosing of RG3039 to 2B/− SMA mice was analyzed at the indicated time points following last dose from (**A**) 20 mg/kg/day P4–P20 dose group, (**B**) a single po dose (20 mg/kg) administered at P11 or (**C**) 2.5 mg/kg/day P4–P20 dose group. The *ex vivo* DcpS inhibition results are shown as thin layer chromatographic analyses and quantified in the corresponding bar graphs. For DcpS *ex vivo* assay, the purified recombinant human DcpS and the radiolabeled m^7Gp^*ppG substrate were used as described previously (23). The authentic radiolabeled product (m^7Gp^*), substrate (m^7Gp^*ppG) marked 'input' as positive controls for DcpS inhibition (cap structure) and a negative vehicle (DMSO) control are shown in lanes 1, 8 and 2, respectively, in (A) and in lanes 1, 2 and 3 in (B) and (C) ($p^* = {}^{32}P$).

RG3039's disease-modifying benefits, it is worth noting that the 5058 Hemi SMA model has also been used to evaluate histone deacetylase inhibitors, one with positive benefit (vorinostat) that had a similar survival increase (30%) as RG3039 and one without (JNJ-26481585) (30,32). While both of those reported studies initiated treatment at birth in 5058 Hemi SMA pups, the treatment with RG3039 in this same model reported here, initiated at this model's midpoint of life (P4) and likely underestimated the survival benefit if treatment had initiated at birth.

Along with the survival and functional advantage, RG3039 tempers motor unit pathology and dysfunction. The histological data with motor neuron counts indicated 2B/− SMA mice have lost 27% of their motor neurons by P18. In RG3039-treated 2B/− SMA mice, there is a trend for attenuation of motor neuron loss that reaches significance in the medial motor neurons. Histological improvements in NMJ innervation and maturity are evident with RG3039 treatment; a finding this is supported by our RNS studies. RG3039 treatment improved neuromuscular transmission as the decrement at 3 Hz was mitigated to 9–18% with an average of 12.6 ± 1.5%, an improvement of ∼37% when compared with vehicle-treated 2B/− SMA mice. Thus, RG3039-treatment improves motor unit pathologies and dysfunction in the remaining motor units. Importantly, in a co-submission with this study, Van Meerbeke *et al.* document similar neurophysiologic improvements as well as survival benefits in delta-7 SMA mice receiving RG3039. Collectively, our work highlights survival benefits across three SMA mouse models and the ability of RG3039 to temper motor unit dysfunction. These are obvious goals for any potential SMA-based therapy. It will be very interesting to

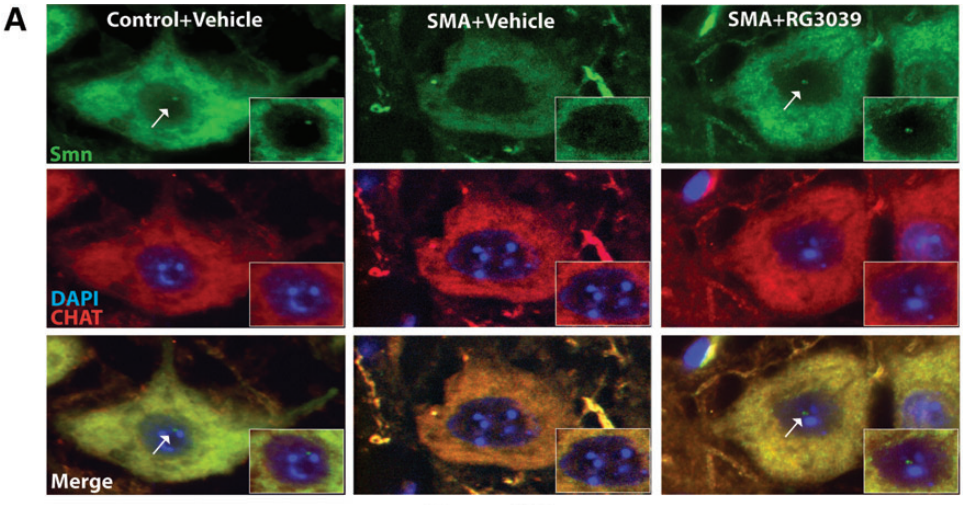

B

Genotype	Avg. Gems per Cell	MNs Counted	MNs with Gems	% MNs With Gems	Number of Cells with 0 Gems	1 Gems	2 Gems	3 Gems	Biological Replicates
Control + Vehicle	0.68 ± 0.03	300	158	52±2%	142	120	31	7	4
SMA + Vehicle	0.20 ± 0.03***	150	44	20±2%***	181	43	1	0	3
SMA + RG3039	0.47 ± 0.03***†††	450	180	40±2%**†††	270	155	20	5	6

Figure 5. RG3039 increases Smn gem number in 2B/− SMA motor neurons. (**A**) Immunofluorescence of ChAT (red) positive motor neurons stained for Smn (green) at P16 from pups treated with vehicle or RG3039 (20 mg/kg) from P4 to P16. Nuclear gems (white arrows) are lost in 2B/− SMA motor neurons and are restored following treatment with RG3039. (**B**) Table quantifying gem number in motor neurons from vehicle-treated at B/+control and 2B/− SMA as well as RG3039-treated 2B/− SMA pups. Data are presented as mean ± SEM. The *P*-values between different treatment cohorts were determined by one-way ANOVA and Bonferroni multiple post hoc comparisons. $^{**}P \leq 0.01$, $^{***}P \leq 0.001$ relative to control; $^{\dagger\dagger\dagger}P \leq 0.001$ relative to 2B/− SMA vehicle.

determine in future studies the effects that RG3039 has in milder SMA mouse models.

Of the available animal models used to test SMA drug candidates preclinically, the delta-7 SMA mouse (28) has been the most widely utilized. It is now accepted that multi-organ systems besides the neuromuscular system impact survival in both the delta-7 and 5058 Hemi SMA mouse models (36,37,39,54–57). The relevance of this to human disease remains to be clarified. The 2B/− SMA mouse also has issues of organ system dysfunction [e.g. liver, kidney, spleen; unpublished and pancreas (58)], but those dysfunctions are slightly delayed in comparison with delta-7 and 5058 Hemi-SMA mice, providing the larger therapeutic window and ability to maximize therapeutic response.

We show here that survival in the 2B/− SMA model can also be used as a primary outcome measure in preclinical drug studies. However, our dose–response data with RG3039 demonstrate that after a certain level of drug administration has been reached, survival and weight gain no longer differentiate dose groups. Thus, the quantitative evaluations of functional outcomes performed at regular intervals that include treadmill walking and gait dynamics with inclined planes at varied angles were built into the study to allow differentiation of the groups (Fig. 3). These evaluations, in addition to survival benefits, provided the discrimination among different dose groups, and thus allowed identification of 2.5 mg/kg as the MED based on survival and function in the 2B/− SMA model. The large difference between the survival of 0.5 and 2.5 mg/kg/day may be the consequence of more than dose proportional change in drug exposure in tissue (by comparison, see Table 3). Further testing would be necessary to observe the decrement in survival and drug exposure with doses between 2.5 and 0.5 mg/kg/day.

Previously, it was reported that DcpS, an RNA cap structure endonuclease, is the target for the C5-substituted 2,4-diaminoquinazoline class of compounds (23), and as we have reported here, RG3039 is a potent DcpS inhibitor. Monitoring *ex vivo* DcpS activity for brain homogenates from the 20 and 2.5 mg/kg dosing studies reported here clearly supports a long PK half-life with an extended PD outcome for RG3039. It was surprising that DcpS inhibition, which has previously been reported to increase Smn protein levels 1.7-fold in delta-7 SMA mice using the closely related compound, D156844, (27), only modestly altered Smn protein levels by western blot in treated 2B/− SMA mice. The analysis of gem number in RG3039-treated motor neurons provided a more robust readout of functional Smn, reaching 75% of control motor neurons. This raises the intriguing possibly that, at least in motor neurons, RG3039 may be introducing a bias in Smn protein localization towards the nucleus, where it is known to play a central role in snRNP assembly.

Overall, the *in vivo* evaluation of RG3039 in 2B/− SMA mice that demonstrated a robust increase in survival (to >600%) along with phenotypic improvements contributed to RG3039 being selected as the clinical candidate. Furthermore, we have demonstrated that drug treatment leads to improvement in gem number in spinal motor neurons following po dosing to 2B/− SMA mice consistent with restoration of RNA metabolism deficits present in Smn-deficient motor neurons.

The collective results, presented above, from survival benefit, motor neuron counts, peripheral NMJ pathology and functional improvement including global improvements in muscle gene

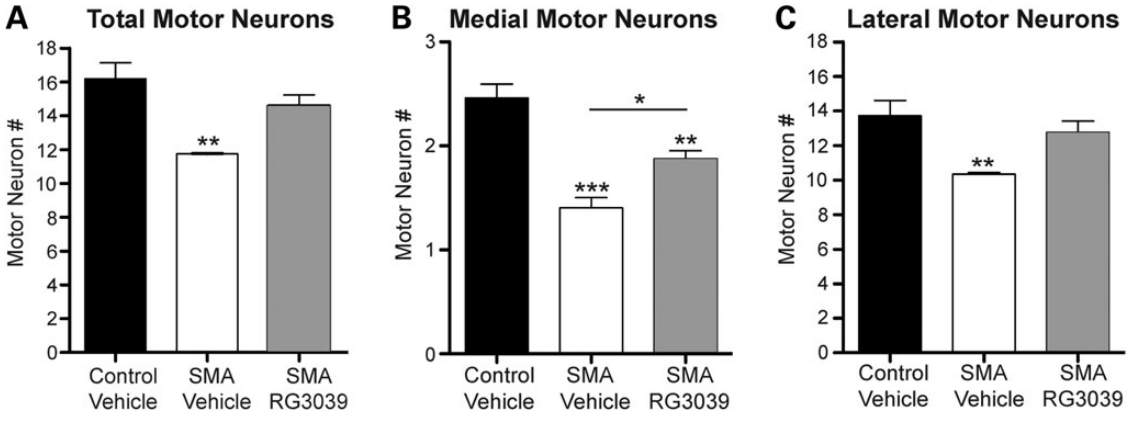

Figure 6. RG3039 attenuates motor neuron loss in 2B/− SMA mice. Motor neuron number was analyzed in cryosections of lumbar spinal cord segments L2–L5 from P16 vehicle-treated control (2B/+) pups (black bars, $n = 4$), vehicle-treated 2B/− SMA mice (white bars, $n = 3$) and RG3039-treated 2B/− SMA pups (gray bars, $n = 6$), which were fluorescently labeled with anti-ChAT antibody. Only ChAT+ neurons with visible nuclei were analyzed. Asterisks show statistical significance ($^{*}P < 0.05$, $^{**}P < 0.01$, $^{***}P < 0.001$) as determined by one-way ANOVA followed by Bonferroni multiple post hoc comparisons. Asterisks above the error bar show significance compared with control, 2B/+ pups (black bars), while asterisks above the line show significance between 2B/− SMA vehicle and RG3039 SMA pups.

expression, suggest RG3039 positively modifies motor unit pathologies and dysfunction. This would indicate that RG3039 alone or in combination with other agents may have therapeutic benefit for SMA.

MATERIALS AND METHODS

Ethics statement

All studies performed on mice were in accordance with the Institutional Animal Care and Use Committee (IACUC) regulations in place at Children's Hospital of Chicago Research Center guidelines and approved under protocols 200920 and 201102.

Animal models

Animals were kept in a controlled vivarium at 25°C and 50% humidity in a 12 h light/12 h dark photoperiod and monitored for health. The Taiwanese SMA mouse model (14), FVB.Cg-Tg*(SMN2)2HungSmn1*^{tm1Hung}*/J* (Jax 5058) are on an FVB/N background and homozygous for both *Tg(SMN2)2Hung* and *Smn1*^{tm1Hung} alleles; hereafter they are referred to as 5058 homozygous mice. They have four copies of *SMN2* (two copies/allele) on an *SmnΔ7* background, live a normal lifespan, are fertile, but develop a necrotic tail shortly after weaning that can extend to the ear pinnae with age. The 5058 Hemi SMA mice used here were generated as described in Gogliotti *et al.* (29). The official name of the *Smn*^{2B} allele is *B6.127-Smn1*$^{tm1.1Cdid}$; hereafter it is referred to as '2B'. It was generated from the progenitor line *Smn*$^{2B\text{-}Neo}$ (*B6.129-Smn1*^{tm1Cdid}) (34) through removal of the flox-neo cassette. Germline mice were subsequently crossed to FVB/NJ mice (Jax stock 001800) for at least three generations prior to use in these studies. FVB/N genetic background was chosen for these studies as the survival curve is non-variable with untreated 2B/− SMA mice dying by 25 days of age and a median survival of ∼20 days. The official name of the *Smn* null allele (*Smn*$^{+/-}$) reported by Schrank *et al.* (35) and used here in a congenic FVBN background is FVB.Cg-*Smn1*^{tm1Msd}. For drug studies using SMA 2B/− mice, intercrosses of *Smn*$^{2B/2B}$ × *Smn*$^{+/-}$ mice were performed to generate offspring in which 50% of the litter were an SMA genotype (2B/−) and 50% were carrier controls (2B/+). For 5058 Hemi and 2B/− SMA crosses, the day of birth was noted as P0. If birth occurred after 3 pm, the following day was noted as P0. At P0, pups were counted. If there were >10 pups to a cage, pups were randomly chosen for culling to reduce litter size to an average of 8. Thereafter, no culling of pups was performed for drug studies.

Drug dosing

For both 5058 Hemi SMA and 2B/− survival studies, test articles for dosing were prepared at Repligen Corporation and then sent in coded vials to the laboratory for testing. The minimum litter size for entry into the drug study was 6 pups and maximum 10. The average litter size in both studies was 8. We were unable to randomize pups within litters to receive drug or vehicle because we determined through PK analysis in WT neonatal mice that drug uptake occurred in the vehicle-treated pups that were within the same cage as those treated with RG3039. Thus, pups within the same cage received only vehicle or drug at a single concentration. To minimize inter-litter variability, we aimed to match litter size and weight between test article groups. All pups were dosed po at 10 μl/g of body weight for vehicle or varying drug concentrations. All neonatal drug studies used water as the vehicle and RG3039 was prepared in water. Only WT adult mice used for PK studies received HPMC vehicle or RG3039 prepared in HPMC.

5058 Hemi SMA dosing

Crosses were performed as described above. At P4, pups were randomized based on weight and dosed with the test article po qd until P11. Each morning mice were monitored for survival, weight, righting reflex and then dosed (in that order). Functional death or severe debilitation of mice was considered to be two consecutive days of weight loss >20% of body weight or an inability to right within 1 min using the righting reflex test. If functional death endpoint was reached requiring euthanasia, that day was noted as death in the survival curve.

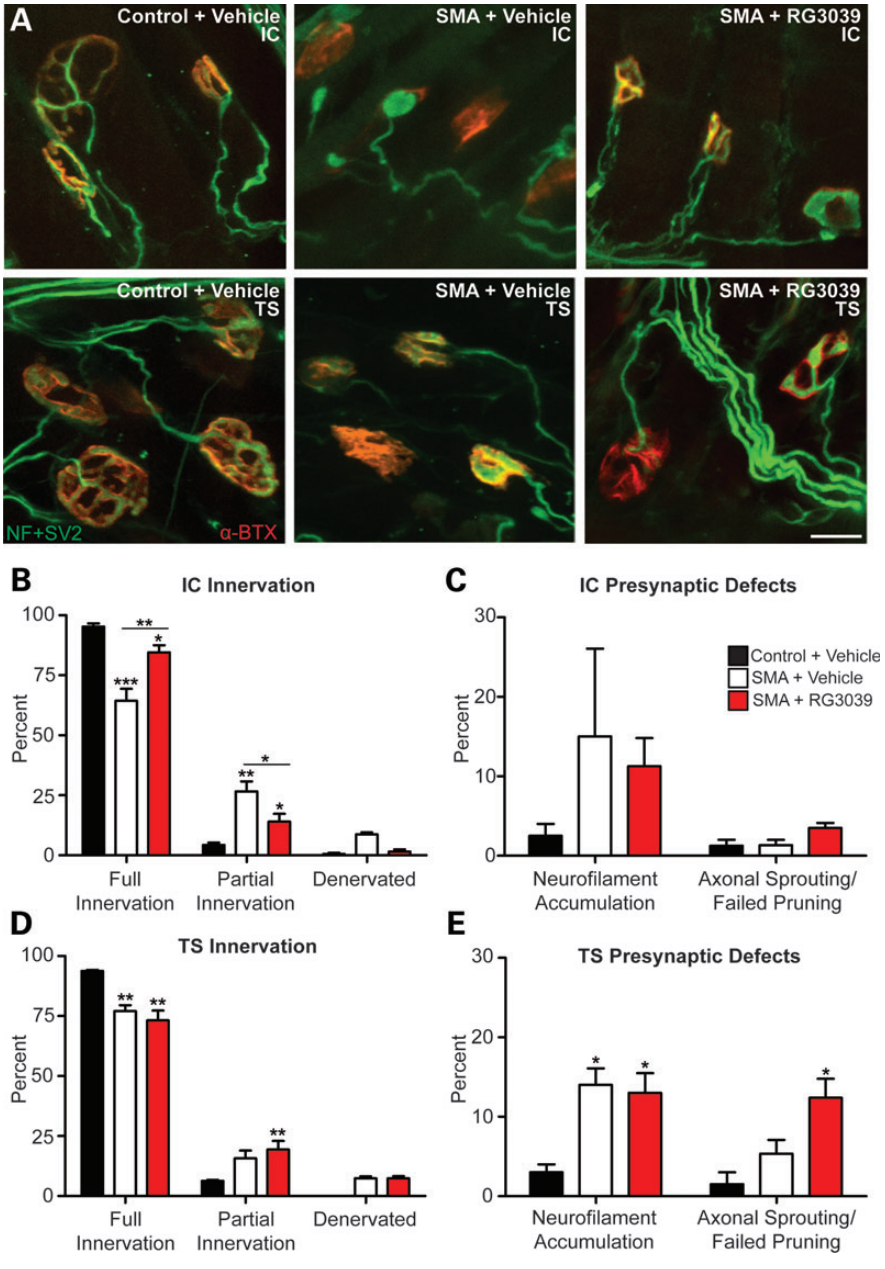

Figure 7. RG3039 improves NMJ pathology and function. 2B/− SMA pups and controls were treated with RG3039 (20 mg/kg) or vehicle from P4 to P18 ($n = 5$/group and $n > 50$ NMJs/pup). (**A**) Whole mount NMJ analysis of IC and TS muscles stained with neurofilament + synaptic vesicle 2 antibodies (green) and α-Bungarotoxin (red) to mark the pre- and post-synaptic junctions. The merged image of the two (yellow) shows the innervation of the muscle and nerve at the motor endplate. Quantification of innervation status of IC (**B**) and TS (**D**) muscles and presynaptic defects in the IC (**C**) and TS (**E**). Post-synaptic endplate maturity as defined in (**F**) was used to quantify vehicle and RG3039-treated IC (**G**) and TS (**H**) NMJ maturity. (**I**) CMAP at P18 measured from the gastrocnemius muscle after nerve stimulation at the sciatic notch from vehicle-treated control (2B/+) pups (black bars, $n = 4$), vehicle-treated 2B/− SMA mice (white bars, $n = 5$) and RG3039-treated 2B/− SMA pups (red bars, $n = 5$). (**J**) CMAPs recorded during RNS showing stable (top, control) decremental response >10% (middle, vehicle SMA) and borderline decremental response of 11% (lower, RG3039 SMA). Untreated/vehicle-treated 2B/− SMA mice ($n = 6$), and RG3039-treated 2B/− SMA pups ($n = 5$). Note asterisks show statistical significance ($^{*}P < 0.05$, $^{**}P < 0.01$, $^{***}P < 0.001$) as determined by two-way ANOVA (A, D, G and H), one-way ANOVA (C, E and I) followed by Bonferroni multiple post hoc comparisons. Asterisks above the error bar show significance compared with control, 2B/+ pups (black bars), while asterisks above the line show significance between 2B/− SMA vehicle and RG3039 2B/− SMA pups.

SMA 2B/− SMA dosing

Similar entry for drug study was used for SMA 2B/− mice as noted above. If litter weight was two standard deviations below the average litter weight of non-treated pups, the litter was not used to avoid the potential of low birth weight affecting survival, phenotypic or pathologic measures. Mice were dosed similarly to 5058 Hemi except from P4 to P20. At P21, all surviving pups were weaned to a maximum of five pups/cage. For each cage of SMA mice, there was one control female kept with the SMA mice. One nesting pad was provided on each cage

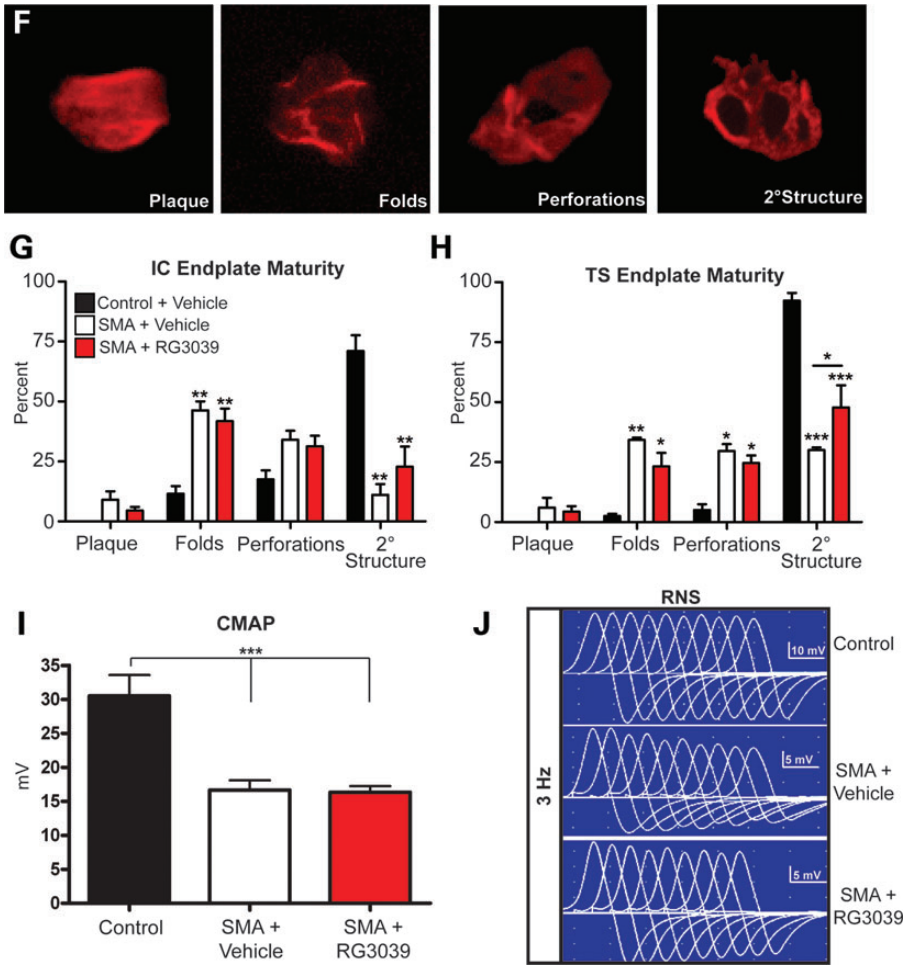

Figure 7. *Continued*

bottom that had SMA mice. As per IACUC regulations, surviving SMA mice were given water-soaked food pellets that were ground to a watery paste and put in one corner of the cage. Cage bottoms of SMA mice were changed 3× week with new food and nesting pad. Phenotypic assays were not performed on the same day to avoid over-exertion and confounding data interpretation. Functional death endpoint was considered to be 30% loss of max body weight or inability to right within 1 min. If this occurred, that day was noted as death in the survival curve portion of the study. Mice were also monitored daily at the time of weight measurement for acute signs of distress that would require euthanasia.

Genotyping

Genotyping of the 5058 Hemi SMA mice was as previously described (29). Genotyping the *Smn* null allele was as previously described (35). The Smn^{2B} allele was typed as previously described in Gogliotti *et al*. (36) with the exception that the neomycin primer was removed from the reaction. Thus, the two primers are a reverse primer, #855 in *Smn* intron 7 (5-gagaccgaggcaggctaac) and a forward primer, #860 within intron 6 (5-tcccaggcagttttagactca). A WT band of 750 bp (Smn^{+}) is amplified and an 850 bp product corresponds to the Smn^{2B} allele. The cycling conditions are 94°C/45 s, 63°C/45 s, 72°C/45 s, 35 cycles.

Phenotyping

Righting reflex was performed as described in (36). If righting did not occur within 1 min, the test was scored a failure. Electrocardiogram (ECG) in conscious unrestrained pups and adults was performed as described in (37,59). Weight was taken daily from P2 to P30 in the morning and thereafter at least five times per week until the study endpoint.

35 and 55° inclined planes: starting at P30 and thereafter every 2 weeks, mice were placed in the center of the incline plane in a face-down position and monitored for their ability to (1) change to an upright position and (2) climb to the top of the inclined platform. Mice were given 1 min to complete the test; otherwise it was scored a failure. A pass in this study dictated a turn from face down to upright and a successful climb to the top of the platform. The platform was placed ∼12 inches off the ground to ensure mice would not walk off the bottom.

High speed ventral plane videography using a DigiGait system (Mouse Specifics, Inc.) was used to generate digital paw prints from which indices of gait were determined as

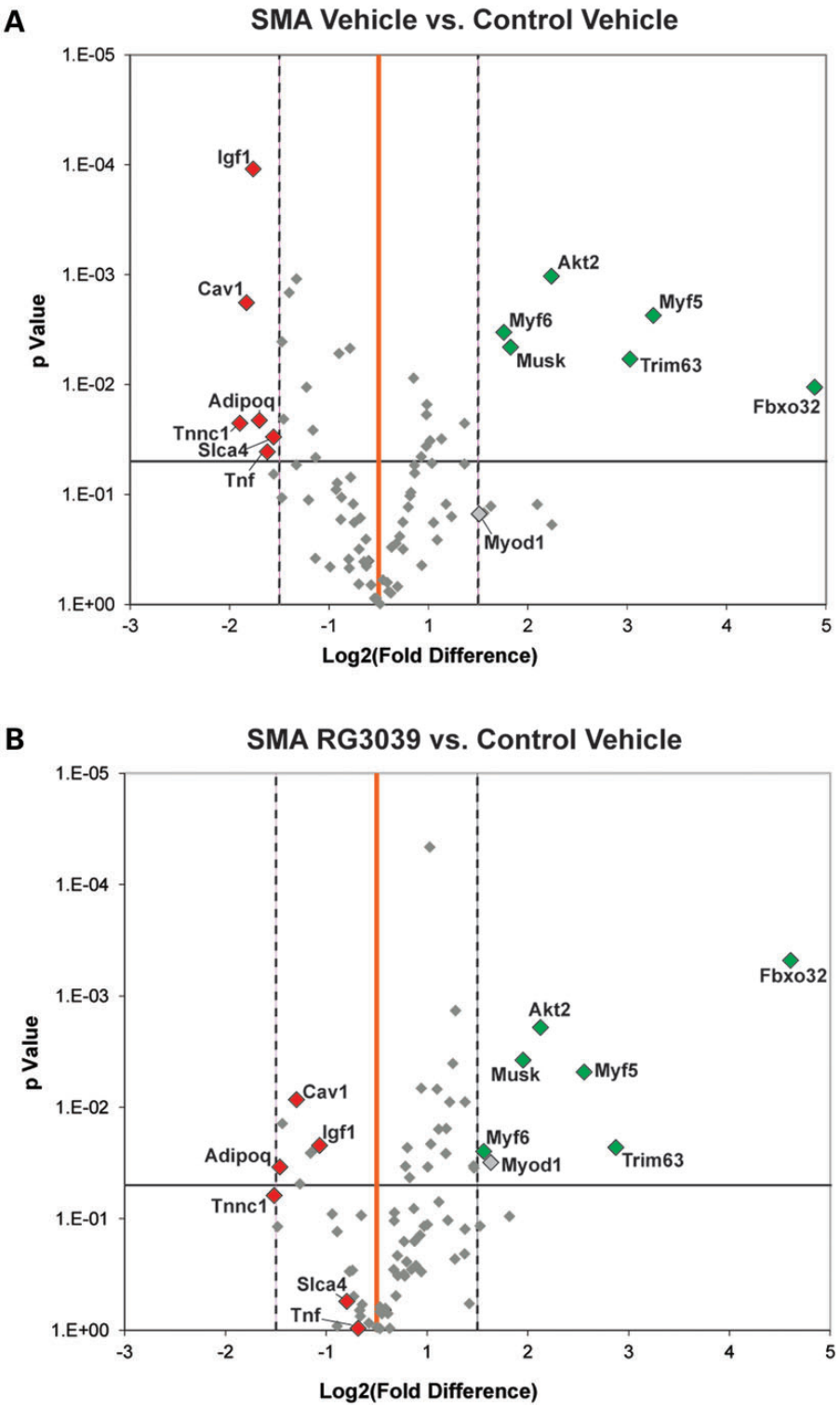

Figure 8. Volcano plots comparing skeletal muscle regeneration and atrophy gene expression fold changes between (**A**) vehicle-treated 2B/− SMA and vehicle-treated control (2B/+) and (**B**) RG3039-treated 2B/− SMA and vehicle-treated control (2B/+). The *X*-axis represents fold change ($\log_2$) and the *Y*-axis *t*-test *P*-value ($-\log_{10}$). The central vertical line (orange) represents a fold value of zero. Each dot represents the expression of a single gene. Dots to the right or left of the dashed vertical lines have a 2-fold increase or decrease, respectively. Dots above the horizontal line indicate significant difference ($P < 0.05$). Those dots shown in color (red; upregulated and green; downregulated) are both significant and expressed $\pm >2$-fold in (A). Vehicle control ($n = 4$); vehicle SMA ($n = 5$); RG3039 ($n = 5$).

previously described (60). Briefly, mice walked on a motor-driven treadmill with a transparent treadmill belt. Images were captured at ∼120 frames per second. Each image represents ∼8 ms. Plotting the area of each digital paw print (paw contact area) imaged sequentially in time provided a dynamic gait signal, representing the temporal record of paw placement

relative to the treadmill belt. Each gait signal comprises a stride duration, which encompasses the swing duration, when the foot is not in contact with the walking surface and the stance duration, when the foot is in contact with the walking surface. Stance can be further divided into braking, the point of first paw contact to maximal paw contact, and propulsion, the point of maximal paw contact to lift-off from the belt surface (shown in Fig. 3E). These measures along with animal placement and measurements of paw positioning relative to the long axis of the mouse can be used to generate paw angle placement, and additional temporal and spatial indices of gait.

Max walking speed in 2B/− SMA mice was determined by initiating walking at 2 cm/s and confirming that the animal was able to sustain that speed for a minimum of 5 s. Speed was increased incrementally with video recording and documentation at each speed using the 5 s threshold. This provided time to rest between each increment. Video was captured at a variety of walking speeds for each mouse over the course of the study. The goal was to capture a minimum of 15 steps for gait analysis for each speed. Comparison of gait between animals and over time was performed on animals walking at the same speed to rule out differences in walking speed as a major confounder to the interpretation of the gait disturbance. Indices for the left and right sides were only pooled if not significantly different to increase the *n*-value for statistical testing between groups. Videos of each mouse were captured once per month.

Western blot analysis

Western blot analysis was performed as previously described (36,37,61) using 5–15 μg of protein per tissue. Detection was performed using the LI-COR Odyssey Imaging System (Biosciences) and quantification was determined using Odyssey Infrared Imaging System Application Software (version 3.0).

Drug formulations

The synthesis of the C5-substituted 2,4-diaminoquinazoline derivative RG3039 (D157495) 5-[[1-(2,6-dichlorobenzyl)piperidin-4-yl]methoxy]quinazoline-2,4-diamine dihydrochloride was completed by Repligen Corporation and the compound was dissolved in water for neonatal studies and HPMC for adult PK studies (Table 1 and Supplementary Material, Fig. S1).

RG3039 DcpS activity assay

Tissue samples were obtained from mice treated with differing doses of RG3039, harvested at the indicated times post-last dose, flash frozen and processed as described in (22) for DcpS activity (23).

RG3039 drug levels

Tissues were homogenized in 0.1% formic acid (1:5 w/v); then 50 μl of homogenate was mixed with 200 μl of acetonitrile spiked with internal standard. After vortexing and centrifugation supernatant was isolated and analyzed. Plasma samples (50 μl) were mixed with 200 μl of acetonitrile spiked with internal standard, vortexed and centrifuged. The supernatants were isolated and analyzed. All samples were analyzed on an LC/MS/MS system consisting of an Agilent 1100 series quaternary pump and micro degasser (Agilent, Santa Clara, CA, USA), a CTC PAL autosampler (Leap Technologies, Carrboro, NC, USA) and an API 4000 triple quadrupole mass spectrometer equipped with an ESI TurboV source (AB Sciex, Foster City, CA, USA). The system is controlled by Analyst 1.4.2 (AB Sciex) running on Windows XP Professional SP3 (Microsoft, Richmond, WA, USA). The API 4000 was operated in positive ESI mode with the following parameters: scan type, MRM; CUR, 30; CAD: 10; IS, 1500; GS1, 60; GS2, 60; TEMP, 400; ihe: ON. MRM transitions were 432.3/256.2 and 382.2/206.2 for RG3039 and the internal standard, respectively, with dwell time of 100 ms for both. An Agilent ZORBAX Eclipse XDB-CN 2.1 × 50 mm 5-μm was used for liquid chromatography. Gradient elution was used with mobile phase A, 25 mM ammonium formate and 0.1% (v/v) formic acid and mobile phase B, 0.1% (v/v) formic acid in acetonitrile. Mobile phase B started at 15%, held for 0.75 min, increased linearly to 50% in 1.75 min, continued to increase linearly to 95% in 1.00 min, held at 95% for 1.00 min, decreased linearly to 15% in 0.10 min and held for 3.40 min. The total run time was 8.00 min and injection volume was 2.5 μl for plasma and 5.0 μl for tissue homogenate. The quantitation was performed by using Analyst 1.4.2 with a calibration curve fitted using a linear regression and $1/x2$ weighting.

Quantitative reverse transcriptase–PCR for gene expression analysis

Hindlimb skeletal muscle was dissected and flash frozen ($n = 5$/group) from vehicle control (2B/+), vehicle 2B/− SMA and RG3039-treated 2B/− SMA mice (20 mg/kg). RNA was prepared using Qiagen reagents and integrity confirmed. mRNA (5 μg/sample) was reverse-transcribed to complementary DNA using the RT^2 First Strand Kit (QIAGEN) according to the manufacturer's instructions. Muscle atrophy and regeneration expression profiles were obtained using PAMM-099 PCR array using SYBR® Green in an ABI 7500 fast cycler. The equivalent to ∼50 ng RNA/well was used and the manufacturer's instructions followed. The expression array contained controls for mouse genomic DNA contamination-, reverse transcription- and positive PCR controls. One control vehicle sample was excluded from data analysis as it failed the positive PCR control. The expression levels of the genes on the array were normalized to four housekeeping genes: GusB, HPRT, HSP90ab1 and Actb, and quantified using the ΔΔ comparative threshold (C_t) method using the analysis tools provided by QIAGEN (http://www.sabiosciences.com/pcr/arrayanalysis.php). IL1b was excluded from analysis as the C_t threshold was >40 in most samples.

Immunofluorescence and NMJ innervation/maturity quantification

NMJ, motor neuron number and gem counts were measured as previously described (36). All NMJs were imaged whole mount on a Leica spinning disk confocal microscope using Slidebook software. Z-stacks were deconvolved in Slidebook and the projection image was used for final analysis. All images

used for analyses were de-identified and randomized prior to quantification for blinding purposes. For NMJs blinded images were assessed for innervation and maturity using Adobe Photoshop, CS4 extended edition. Innervation status was defined visually as fully innervated (>80%), partially innervated (15–80%) or denervated (<15%). Post-synaptic maturity was defined as junctions containing homogeneous plaques, folds, perforations or secondary structure. Only after quantification was complete were the images re-identified for analysis.

Neurophysiology

Electrophysiological recordings were performed on control and SMA using a Synergy electromyography unit. Mice were briefly anesthetized using isoflurane (3%) and then decreased to 1.5% for the remainder of the study. Body temperature was maintained with a heating lamp. CMAP amplitudes in the sciatic innervated calf gastrocnemius muscle were obtained after electric stimulation at the sciatic notch. Subdermal needle electrodes were inserted in the sciatic notch for stimulation and ring electrodes placed around the gastrocnemius muscle and distal tendon at the ankle were used to record CMAP amplitude. Peak-to-peak amplitudes (mV), duration (time needed between depolarization and repolarization sessions) and motor latencies (ms) were recorded from the gastrocnemius. RNS was performed after a single super-maximal stimulation was determined. Then, a train of stimuli at 3, 10 and 20 Hz was applied and the resulting CMAPs recorded.

Statistical analysis

Data were presented as the average ± SEM, unless otherwise stated. Statistical analyses were performed using Graph Pad Prism software (version 4.0). Kaplan–Meier survival curves were generated from the data and compared using Mantel–Cox log-rank test. Significance in weights, innervation status and post-synaptic maturity was determined using two-way analysis of variance (ANOVA) with a Bonferroni post hoc comparison. Significance pertaining to motor neuron counts and heart rate was analyzed with a Student's *t*-test if only comparing two samples or one-way ANOVA, with Bonferroni post hoc comparisons if comparing against multiple groups.

SUPPLEMENTARY MATERIAL

Supplementary Material is available at *HMG* online.

ACKNOWLEDGEMENTS

The authors gratefully acknowledge the scientific contributions of Jon M. Bjornsson and Margrét Thorsteinsdóttir from deCode genetics, Reykjavik, Iceland.

Conflict of Interest statement. J.J. is an employee of Families of SMA and has no financial interest in the project or compound tested. Families of SMA has a financial interest in the compound tested. Families of SMA supported a portion of these studies. Heather Plasterer, B.X., V.J. and J.R. were employees of Repligen Corporation during the design and execution of these studies. These authors hold non-controlling shares in Repligen Corporation. Repligen supported a portion of these studies. Repligen Corporation has a financial interest in the compound tested. All other authors have no conflict of interest. Both Families of SMA and Repligen participated in the study design. The manuscript was written by C.J.D., J.S. and R.G.G. All authors participated in revisions of the manuscript.

FUNDING

This work was supported by funding from the Families of SMA and Repligen Corporation. Repligen Corporation received funding from the Muscular Dystrophy Association. In addition, C.J.D. was supported by National Institutes of Health (1RO1NS060926-04 and 5R21 NS067482-02) and M.K. was supported by the Families of SMA. C.E. and R.G.G. were supported by the National Institutes of Health training grants (5T32GM008061) and (T32 AG000260), respectively. Families of SMA financially supported and directed the identification and generation of the quinazoline series of compounds, including RG3039.

REFERENCES

1. Crawford, T.O. and Pardo, C.A. (1996) The neurobiology of childhood spinal muscular atrophy. *Neurobiol. Dis.*, **3**, 97–110.
2. Pearn, J. (1978) Incidence, prevalence, and gene frequency studies of chronic childhood spinal muscular atrophy. *J. Med. Genet.*, **15**, 409–413.
3. Feldkotter, M., Schwarzer, V., Wirth, R., Wienker, T.F. and Wirth, B. (2002) Quantitative analyses of SMN1 and SMN2 based on real-time lightCycler PCR: fast and highly reliable carrier testing and prediction of severity of spinal muscular atrophy. *Am. J. Hum. Genet.*, **70**, 358–368.
4. Munsat, T.L. and Davies, K.E. (1992) International SMA consortium meeting (26–28 June 1992, Bonn, Germany). *Neuromuscul. Disord.*, **2**, 423–428.
5. Zerres, K. and Rudnik-Schoneborn, S. (1995) Natural history in proximal spinal muscular atrophy. Clinical analysis of 445 patients and suggestions for a modification of existing classifications. *Arch. Neurol.*, **52**, 518–523.
6. Wang, C.H., Finkel, R.S., Bertini, E.S., Schroth, M., Simonds, A., Wong, B., Aloysius, A., Morrison, L., Main, M., Crawford, T.O. *et al.* (2007) Consensus statement for standard of care in spinal muscular atrophy. *J. Child Neurol.*, **22**, 1027–1049.
7. Lefebvre, S., Burglen, L., Reboullet, S., Clermont, O., Burlet, P., Viollet, L., Benichou, B., Cruaud, C., Millasseau, P., Zeviani, M. *et al.* (1995) Identification and characterization of a spinal muscular atrophy-determining gene. *Cell*, **80**, 155–165.
8. Wirth, B. (2000) An update of the mutation spectrum of the survival motor neuron gene (SMN1) in autosomal recessive spinal muscular atrophy (SMA). *Hum. Mutat.*, **15**, 228–237.
9. Lorson, C.L., Hahnen, E., Androphy, E.J. and Wirth, B. (1999) A single nucleotide in the SMN gene regulates splicing and is responsible for spinal muscular atrophy. *Proc. Natl Acad. Sci. USA*, **96**, 6307–6311.
10. Monani, U.R., Lorson, C.L., Parsons, D.W., Prior, T.W., Androphy, E.J., Burghes, A.H. and McPherson, J.D. (1999) A single nucleotide difference that alters splicing patterns distinguishes the SMA gene SMN1 from the copy gene SMN2. *Hum. Mol. Genet.*, **8**, 1177–1183.
11. Lorson, C.L. and Androphy, E.J. (2000) An exonic enhancer is required for inclusion of an essential exon in the SMA-determining gene SMN. *Hum. Mol. Genet.*, **9**, 259–265.
12. McAndrew, P.E., Parsons, D.W., Simard, L.R., Rochette, C., Ray, P.N., Mendell, J.R., Prior, T.W. and Burghes, A.H. (1997) Identification of proximal spinal muscular atrophy carriers and patients by analysis of SMNT and SMNC gene copy number. *Am. J. Hum. Genet.*, **60**, 1411–1422.
13. Coovert, D.D., Le, T.T., McAndrew, P.E., Strasswimmer, J., Crawford, T.O., Mendell, J.R., Coulson, S.E., Androphy, E.J., Prior, T.W. and Burghes, A.H. (1997) The survival motor neuron protein in spinal muscular atrophy. *Hum. Mol. Genet.*, **6**, 1205–1214.

14. Hsieh-Li, H.M., Chang, J.G., Jong, Y.J., Wu, M.H., Wang, N.M., Tsai, C.H. and Li, H. (2000) A mouse model for spinal muscular atrophy. *Nat. Genet.*, **24**, 66–70.
15. Jarecki, J., Chen, X., Bernardino, A., Coovert, D.D., Whitney, M., Burghes, A., Stack, J. and Pollok, B.A. (2005) Diverse small-molecule modulators of SMN expression found by high-throughput compound screening: early leads towards a therapeutic for spinal muscular atrophy. *Hum. Mol. Genet.*, **14**, 2003–2018.
16. Mattis, V.B., Rai, R., Wang, J., Chang, C.W., Coady, T. and Lorson, C.L. (2006) Novel aminoglycosides increase SMN levels in spinal muscular atrophy fibroblasts. *Hum. Genet.*, **120**, 589–601.
17. Hahnen, E., Eyupoglu, I.Y., Brichta, L., Haastert, K., Trankle, C., Siebzehnrubl, F.A., Riessland, M., Holker, I., Claus, P., Romstock, J. *et al.* (2006) *In vitro* and *ex vivo* evaluation of second-generation histone deacetylase inhibitors for the treatment of spinal muscular atrophy. *J. Neurochem.*, **98**, 193–202.
18. Makhortova, N.R., Hayhurst, M., Cerqueira, A., Sinor-Anderson, A.D., Zhao, W.N., Heiser, P.W., Arvanites, A.C., Davidow, L.S., Waldon, Z.O., Steen, J.A. *et al.* (2011) A screen for regulators of survival of motor neuron protein levels. *Nat. Chem. Biol.*, **7**, 544–552.
19. Xiao, J., Marugan, J.J., Zheng, W., Titus, S., Southall, N., Cherry, J.J., Evans, M., Androphy, E.J. and Austin, C.P. (2011) Discovery, synthesis, and biological evaluation of novel SMN protein modulators. *J. Med. Chem.*, **54**, 6215–6233.
20. Cherry, J.J. and Androphy, E.J. (2012) Therapeutic strategies for the treatment of spinal muscular atrophy. *Future Med. Chem.*, **4**, 1733–1750.
21. Lorson, M.A. and Lorson, C.L. (2012) SMN-inducing compounds for the treatment of spinal muscular atrophy. *Future Med. Chem.*, **4**, 2067–2084.
22. Thurmond, J., Butchbach, M.E., Palomo, M., Pease, B., Rao, M., Bedell, L., Keyvan, M., Pai, G., Mishra, R., Haraldsson, M. *et al.* (2008) Synthesis and biological evaluation of novel 2,4-diaminoquinazoline derivatives as SMN2 promoter activators for the potential treatment of spinal muscular atrophy. *J. Med. Chem.*, **51**, 449–469.
23. Singh, J., Salcius, M., Liu, S.W., Staker, B.L., Mishra, R., Thurmond, J., Michaud, G., Mattoon, D.R., Printen, J., Christensen, J. *et al.* (2008) DcpS as a therapeutic target for spinal muscular atrophy. *ACS Chem. Biol.*, **3**, 711–722.
24. Bail, S. and Kiledjian, M. (2008) DcpS, a general modulator of cap-binding protein-dependent processes? *RNA Biol.*, **5**, 216–219.
25. Shen, V., Liu, H., Liu, S.W., Jiao, X. and Kiledjian, M. (2008) DcpS scavenger decapping enzyme can modulate pre-mRNA splicing. *RNA*, **14**, 1132–1142.
26. Liu, H., Rodgers, N.D., Jiao, X. and Kiledjian, M. (2002) The scavenger mRNA decapping enzyme DcpS is a member of the HIT family of pyrophosphatases. *EMBO J.*, **21**, 4699–4708.
27. Butchbach, M.E., Singh, J., Thorsteinsdottir, M., Saieva, L., Slominski, E., Thurmond, J., Andresson, T., Zhang, J., Edwards, J.D., Simard, L.R. *et al.* (2010) Effects of 2,4-diaminoquinazoline derivatives on SMN expression and phenotype in a mouse model for spinal muscular atrophy. *Hum. Mol. Genet.*, **19**, 454–467.
28. Le, T.T., Pham, L.T., Butchbach, M.E., Zhang, H.L., Monani, U.R., Coovert, D.D., Gavrilina, T.O., Xing, L., Bassell, G.J. and Burghes, A.H. (2005) SMNDelta7, the major product of the centromeric survival motor neuron (SMN2) gene, extends survival in mice with spinal muscular atrophy and associates with full-length SMN. *Hum. Mol. Genet.*, **14**, 845–857.
29. Gogliotti, R.G., Hammond, S.M., Lutz, C. and DiDonato, C.J. (2010) Molecular and phenotypic reassessment of an infrequently used mouse model for spinal muscular atrophy. *Biochem. Biophys. Res. Commun.*, **391**, 517–522.
30. Riessland, M., Ackermann, B., Forster, A., Jakubik, M., Hauke, J., Garbes, L., Fritzsche, I., Mende, Y., Blumcke, I., Hahnen, E. *et al.* (2010) SAHA ameliorates the SMA phenotype in two mouse models for spinal muscular atrophy. *Hum. Mol. Genet.*, **19**, 1492–1506.
31. Hua, Y., Sahashi, K., Rigo, F., Hung, G., Horev, G., Bennett, C.F. and Krainer, A.R. (2011) Peripheral SMN restoration is essential for long-term rescue of a severe spinal muscular atrophy mouse model. *Nature*, **478**, 123–126.
32. Schreml, J., Riessland, M., Paterno, M., Garbes, L., Rossbach, K., Ackermann, B., Kramer, J., Somers, E., Parson, S.H., Heller, R. *et al.* (2012) Severe SMA mice show organ impairment that cannot be rescued by therapy with the HDACi JNJ-26481585. *Eur. J. Hum. Genet.*, 17 October. doi:10.1038/ejhg.2012.222.
33. Bowerman, M., Murray, L.M., Beauvais, A., Pinheiro, B. and Kothary, R. (2012) A critical smn threshold in mice dictates onset of an intermediate spinal muscular atrophy phenotype associated with a distinct neuromuscular junction pathology. *Neuromuscul. Disord.*, **22**, 263–276.
34. Hammond, S.M., Gogliotti, R.G., Rao, V., Beauvais, A., Kothary, R. and DiDonato, C.J. (2010) Mouse survival motor neuron alleles that mimic SMN2 splicing and are inducible rescue embryonic lethality early in development but not late. *PloS One*, **5**, e15887.
35. Schrank, B., Gotz, R., Gunnersen, J.M., Ure, J.M., Toyka, K.V., Smith, A.G. and Sendtner, M. (1997) Inactivation of the survival motor neuron gene, a candidate gene for human spinal muscular atrophy, leads to massive cell death in early mouse embryos. *Proc. Natl Acad. Sci. USA*, **94**, 9920–9925.
36. Gogliotti, R.G., Quinlan, K.A., Barlow, C.B., Heier, C.R., Heckman, C.J. and DiDonato, C.J. (2012) Motor neuron rescue in spinal muscular atrophy mice demonstrates that sensory-motor defects are a consequence, not a cause, of motor neuron dysfunction. *J. Neurol.*, **32**, 3818–3829.
37. Heier, C.R., Satta, R., Lutz, C. and DiDonato, C.J. (2010) Arrhythmia and cardiac defects are a feature of spinal muscular atrophy model mice. *Hum. Mol. Genet.*, **19**, 3906–3920.
38. Porensky, P.N., Mitrpant, C., McGovern, V.L., Bevan, A.K., Foust, K.D., Kaspar, B.K., Wilton, S.D. and Burghes, A.H. (2012) A single administration of morpholino antisense oligomer rescues spinal muscular atrophy in mouse. *Hum. Mol. Genet.*, **21**, 1625–1638.
39. Bevan, A.K., Hutchinson, K.R., Foust, K.D., Braun, L., McGovern, V.L., Schmelzer, L., Ward, J.G., Petruska, J.C., Lucchesi, P.A., Burghes, A.H. *et al.* (2010) Early heart failure in the SMNΔ7 model of spinal muscular atrophy and correction by postnatal scAAV9-SMN delivery. *Hum. Mol. Genet.*, **19**, 3895–3905.
40. Liu, Q. and Dreyfuss, G. (1996) A novel nuclear structure containing the survival of motor neurons protein. *EMBO J.*, **15**, 3555–3565.
41. Andreassi, C., Jarecki, J., Zhou, J., Coovert, D.D., Monani, U.R., Chen, X., Whitney, M., Pollok, B., Zhang, M., Androphy, E. *et al.* (2001) Aclarubicin treatment restores SMN levels to cells derived from type I spinal muscular atrophy patients. *Hum. Mol. Genet.*, **10**, 2841–2849.
42. Kariya, S., Park, G.H., Maeno-Hikichi, Y., Leykekhman, O., Lutz, C., Arkovitz, M.S., Landmesser, L.T. and Monani, U.R. (2008) Reduced SMN protein impairs maturation of the neuromuscular junctions in mouse models of spinal muscular atrophy. *Hum. Mol. Genet.*, **17**, 2552–2569.
43. Kong, L., Wang, X., Choe, D.W., Polley, M., Burnett, B.G., Bosch-Marce, M., Griffin, J.W., Rich, M.M. and Sumner, C.J. (2009) Impaired synaptic vesicle release and immaturity of neuromuscular junctions in spinal muscular atrophy mice. *J. Neurol.*, **29**, 842–851.
44. Monani, U.R., Sendtner, M., Coovert, D.D., Parsons, D.W., Andreassi, C., Le, T.T., Jablonka, S., Schrank, B., Rossol, W., Prior, T.W. *et al.* (2000) The human centromeric survival motor neuron gene (SMN2) rescues embryonic lethality in Smn(−/−) mice and results in a mouse with spinal muscular atrophy. *Hum. Mol. Genet.*, **9**, 333–339.
45. Murray, L.M., Comley, L.H., Thomson, D., Parkinson, N., Talbot, K. and Gillingwater, T.H. (2008) Selective vulnerability of motor neurons and dissociation of pre- and post-synaptic pathology at the neuromuscular junction in mouse models of spinal muscular atrophy. *Hum. Mol. Genet.*, **17**, 949–962.
46. Mentis, G.Z., Blivis, D., Liu, W., Drobac, E., Crowder, M.E., Kong, L., Alvarez, F.J., Sumner, C.J. and O'Donovan, M.J. (2011) Early functional impairment of sensory-motor connectivity in a mouse model of spinal muscular atrophy. *Neuron*, **69**, 453–467.
47. Avila, A.M., Burnett, B.G., Taye, A.A., Gabanella, F., Knight, M.A., Hartenstein, P., Cizman, Z., Di Prospero, N.A., Pellizzoni, L., Fischbeck, K.H. *et al.* (2007) Trichostatin A increases SMN expression and survival in a mouse model of spinal muscular atrophy. *J. Clin. Invest.*, **117**, 659–671.
48. Farooq, F., Molina, F.A., Hadwen, J., MacKenzie, D., Witherspoon, L., Osmond, M., Holcik, M. and MacKenzie, A. (2011) Prolactin increases SMN expression and survival in a mouse model of severe spinal muscular atrophy via the STAT5 pathway. *J. Clin. Invest.*, **121**, 3042–3050.
49. Hastings, M.L., Berniac, J., Liu, Y.H., Abato, P., Jodelka, F.M., Barthel, L., Kumar, S., Dudley, C., Nelson, M., Larson, K. *et al.* (2009) Tetracyclines that promote SMN2 exon 7 splicing as therapeutics for spinal muscular atrophy. *Sci. Transl. Med.*, **1**, 5ra12.
50. Le, T.T., McGovern, V.L., Alwine, I.E., Wang, X., Massoni-Laporte, A., Rich, M.M. and Burghes, A.H. (2011) Temporal requirement for high SMN expression in SMA mice. *Hum. Mol. Genet.*, **20**, 3578–3591.
51. Lutz, C.M., Kariya, S., Patruni, S., Osborne, M.A., Liu, D., Henderson, C.E., Li, D.K., Pellizzoni, L., Rojas, J., Valenzuela, D.M. *et al.* (2011)

Postsymptomatic restoration of SMN rescues the disease phenotype in a mouse model of severe spinal muscular atrophy. *J. Clin. Invest.*, **121**, 3029–3041.
52. Passini, M.A., Bu, J., Richards, A.M., Kinnecom, C., Sardi, S.P., Stanek, L.M., Hua, Y., Rigo, F., Matson, J., Hung, G. *et al.* (2011) Antisense oligonucleotides delivered to the mouse CNS ameliorate symptoms of severe spinal muscular atrophy. *Sci. Transl. Med.*, **3**, 72ra18.
53. Passini, M.A., Bu, J., Roskelley, E.M., Richards, A.M., Sardi, S.P., O'Riordan, C.R., Klinger, K.W., Shihabuddin, L.S. and Cheng, S.H. (2010) CNS-targeted gene therapy improves survival and motor function in a mouse model of spinal muscular atrophy. *J. Clin. Invest.*, **120**, 1253–1264.
54. Shababi, M., Habibi, J., Yang, H.T., Vale, S.M., Sewell, W.A. and Lorson, C.L. (2010) Cardiac defects contribute to the pathology of spinal muscular atrophy models. *Hum. Mol. Genet.*, **19**, 4059–4071.
55. Somers, E., Stencel, Z., Wishart, T.M., Gillingwater, T.H. and Parson, S.H. (2012) Density, calibre and ramification of muscle capillaries are altered in a mouse model of severe spinal muscular atrophy. *Neuromuscul. Disord.*, **22**, 435–442.
56. Wishart, T.M., Huang, J.P., Murray, L.M., Lamont, D.J., Mutsaers, C.A., Ross, J., Geldsetzer, P., Ansorge, O., Talbot, K., Parson, S.H. *et al.* (2010) SMN deficiency disrupts brain development in a mouse model of severe spinal muscular atrophy. *Hum. Mol. Genet.*, **19**, 4216–4228.
57. Mutsaers, C.A., Wishart, T.M., Lamont, D.J., Riessland, M., Schreml, J., Comley, L.H., Murray, L.M., Parson, S.H., Lochmuller, H., Wirth, B. *et al.* (2011) Reversible molecular pathology of skeletal muscle in spinal muscular atrophy. *Hum. Mol. Genet.*, **20**, 4334–4344.
58. Bowerman, M., Swoboda, K.J., Michalski, J.P., Wang, G.S., Reeks, C., Beauvais, A., Murphy, K., Woulfe, J., Screaton, R.A., Scott, F.W. *et al.* (2012) Glucose metabolism and pancreatic defects in spinal muscular atrophy. *Ann. Neurol.*, **72**, 256–268.
59. Heier, C.R., Hampton, T.G., Wang, D. and DiDonato, C.J. (2010) Development of electrocardiogram intervals during growth of FVB/N neonate mice. *BMC Physiol.*, **10**, 16.
60. Hampton, T.G., Stasko, M.R., Kale, A., Amende, I. and Costa, A.C. (2004) Gait dynamics in trisomic mice: quantitative neurological traits of Down syndrome. *Physiol. Behav.*, **82**, 381–389.
61. Gogliotti, R.G., Lutz, C., Jorgensen, M., Huebsch, K., Koh, S. and DiDonato, C.J. (2011) Characterization of a commonly used mouse model of SMA reveals increased seizure susceptibility and heightened fear response in FVB/N mice. *Neurobiol. Dis.*, **43**, 142–151.